Supporting Information

More is Different: Progressive *β*-Thiolation Induced-Porphyrin Aggregation Switches Singlet Oxygen Photosensitization

Mengliang Zhu[+],[a,b] Hang Zhang[+],[a] Yuhang Yao[+],[a] Mingpu Wen,[c] Guangliu Ran,[d] Yi Yu,[a] Ruijing Zhang,[a] Xing-Jie Liang,[b,e] Jing Zhang,[c] Wenkai Zhang,*[d] and Jun-Long Zhang*[a]

[a] *Beijing National Laboratory for Molecular Sciences, College of Chemistry and Molecular Engineering, Peking University, Beijing 100871, P. R. China.*

[b] *CAS Key Laboratory for Biomedical Effects of Nanomaterials and Nanosafety, CAS Center for Excellence in Nanoscience, National Center for Nanoscience and Technology of China, Beijing 100190, P. R. China.*

[c] *College of Materials Science and Opto-Electronic Technology, University of Chinese Academy of Sciences, Beijing 100049, P. R. China.*

[d] *Center for Advanced Quantum Studies, Department of Physics and Applied Optics Beijing Area Major Laboratory, Beijing Normal University, Beijing 100875, P. R. China.*

[e] *University of Chinese Academy of Sciences. Beijing 100049, P. R. China.*

[+] *These authors contributed equally to this work.*

* *Correspondence to: Jun-long Zhang, e-mail: zhangjunlong@pku.edu.cn*;

Wenkai Zhang, e-mail: wkzhang@bnu.edu.cn.

Contents

Chemicals and instruments

Column chromatography was carried out on silica gel (200-300 mesh, Qingdao Ocean Chemicals) with the indicated eluents. All other reagents and solvents were used as received. 5,10,15,20-tetra(pentafluorophenyl)porphodilactone was synthesized according to literature methods.[1] ^{1}H and ^{19}F NMR spectra were recorded using a Bruker DPX 400 MHz spectrometer and the chemical shifts were reported relative to internal $SiMe_4$. ESI mass spectra were recorded using a Bruker APEX IV FTICR mass spectrometer. Electronic absorption spectra were recorded using an Agilent 8453 UV/Vis spectrometer. The fluorescence emission spectra were recorded using an Edinburgh FLS980 spectrometer. Transmission electron microscope (TEM) measurements were performed using a JEOL JEM-2100F field-emission high resolution transmission electron microscope operated at 200 kV. The size distribution of the NPs in aqueous solution were measured using a Brookhaven Zeta potential and particle size analyzer (90 Plus Zeta). fs-TA spectra were recorded in HARPIA spectrometer equipped with a PHAROS femtosecond laser. ns-TA spectra were recorded using an Edinburgh LP980 spectrometer combined with a Nd: YAG laser. Confocal fluorescence microscopy was performed using an ISS Alba5 FLIM/FFS confocal system equipped with a Nikon TE2000 inverted microscope. *In vitro* and *in vivo* PDT was performed using PURI Materials cellular phototoxicity (small animal phototherapy) irradiators equipped with LED light (700 nm).

Synthesis and characterization

Synthesis of porphothiodilactone. Porphodilactone (100 mg, 0.10 mmol), Lawesson's reagent (20 equiv., 1.00 g, 2.0 mmol) were dissolved in 10 mL anhydrous toluene. The mixture was refluxed under nitrogen for 3 days in the dark. After that the reaction mixture was cooled down to room temperature, and the residue was purified by column chromatography on silica gel using DCM/petroleum ether (1:10) as eluent. The S-substituted products of *trans*/*cis*-porphodilactone with different S atom numbers (termed by ***trans*-S'S**, ***trans*-O'S**, ***cis*-S'S** and ***cis*-O'S**) were eluted in sequence.

***trans*-S'S**: Yield: 15%. ^{1}H NMR ($CDCl_3$, 400 MHz): δ 8.70 (s, 4H), −0.98 (s, 2H). ^{19}F NMR ($CDCl_3$, 471 MHz): δ −136.83 ~ −136.89 (m, 4F), −138.29 ~ −138.35 (m, 4F), −149.38 (t, J = 21.2 Hz, 2F), −151.14 (t, J = 20.7 Hz, 2F), −159.97 ~ −160.08 (m, 4F), −160.68 ~ −160.78 (m, 4F). HR-MS (ESI^+) m/z $[M+H]^+$: Calcd for $C_{42}H_7F_{20}N_4O_2S_2$ 1042.9686; found: 1042.9669.

***trans*-O'S**: Yield: 20%. ^{1}H NMR ($CDCl_3$, 400 MHz): δ 8.81 ~ 8.75 (m, 4H), −1.52 (s, 1H), -1.57 (s, 1H). ^{19}F NMR ($CDCl_3$, 471 MHz): δ −136.83 ~ −137.03 (m, 4F), −138.32 ~ −138.49 (m, 4F), −149.37 (t, J = 20.7 Hz, 1F), −149.52 (t, J = 20.7 Hz, 1F), −150.27 (t, J = 21.2 Hz, 1F), −151.22 (t, J = 20.7 Hz, 1F), −160.00 ~ −160.27 (m, 4F), −160.75 ~ −160.90 (m, 4F). HR-MS (ESI$^+$) m/z [M+H]$^+$: Calcd for $C_{42}H_7F_{20}N_4O_3S$ 1026.9914; found: 1026.9889.

***cis*-S'S**: Yield: 15%. ^{1}H NMR ($CDCl_3$, 400 MHz): δ 8.59 (s, 2H), 8.42 (s, 2H), 0.64 (s, 1H), −0.13 (s, 1H). ^{19}F NMR ($CDCl_3$, 471 MHz): δ −136.90 ~ −136.94 (m, 4F), −138.66 ~ −138.73 (m, 4F), −149.33 (t, J = 20.7 Hz, 2F), −151.27 (t, J = 20.7 Hz, 2F), −159.86 ~ −159.96 (m, 4F), −160.59 ~ −160.69 (m, 4F). HR-MS (ESI$^+$) m/z [M+H]$^+$: Calcd for $C_{42}H_7F_{20}N_4O_2S_2$ 1042.9686; found: 1042.9683.

***cis*-O'S**: Yield: 20%. ^{1}H NMR ($CDCl_3$, 400 MHz): δ 8.65 (d, J = 10.4 Hz, 2H), 8.51 (s, 1H), 8.45 (s, 1H), 0.16 (s, 1H), −0.52 (s, 1H). ^{19}F NMR ($CDCl_3$, 471 MHz): δ −136.90 ~ −137.07 (m, 4F), −138.63 ~ −138.75 (m, 4F), −149.30 ~ −149.49 (m, 2F), −150.43 (t, J = 20.7 Hz, 1F), −151.35 (t, J = 20.7 Hz, 1F), −159.91 ~ −160.14 (m, 4F), −160.65 ~ −160.89 (m, 4F). HR-MS (ESI$^+$) m/z [M+H]$^+$: Calcd for $C_{42}H_7F_{20}N_4O_3S$ 1026.9914; found: 1026.9898.

Measurement of fluorescence quantum yields (Φ_{em})

The fluorescence quantum yields were determined by the equation $\Phi_{em}^{s} = \Phi_{em}^{r}(I_{em}^{s}A_r n_s^2)/(I_{em}^{r}A_s n_r^2)$, where the super/subscripts *s* and *r* refer to the sample and the reference compound, respectively. Tetraphenylporphyrin (**TPP**) was used as the reference (Φ_{em} = 0.11, in CH_2Cl_2).[2] Φ_{em} is the fluorescence quantum yield, I_{em} is the integrated fluorescence emission intensity, A is the absorbance at the excitation wavelength, n is the refractive index of the solvent. In all measurements, the steady state fluorescence emission spectra were obtained using an excitation at 405 nm with absorbance ranged between 0.01 and 0.05 at room temperature.

Measurement of singlet oxygen quantum yields (Φ_Δ)

Measurements were taken at 405 nm excitation in air-saturated solutions at room temperature with **TPP** (Φ_Δ = 0.55) in $CHCl_3$ as reference,[3] by comparing the intensity of singlet oxygen phosphorescence emission at 1275 nm measured with a FLS980

spectrofluorimeter (Edinburgh). The singlet oxygen quantum yields were calculated by using equation $\Phi_{\Delta}^{s} = \Phi_{\Delta}^{r}(I_{\Delta}^{s}A_{r}n_{s}^{2})/(I_{\Delta}^{r}A_{s}n_{r}^{2})$, where the super/subscripts *s* and *r* refer to the sample and the reference compound, respectively. Φ_{Δ} is the singlet oxygen quantum yield, I_{Δ} is the integrated intensity of singlet oxygen phosphorescence emission, *A* is the absorbance at the excitation wavelength, *n* is the refractive index of the solvent. The absorbance at the excited wavelength (405 nm, typically adjusted to 0.1), respectively.

SOSG assay for singlet oxygen

SOSG (5 μM) was added into 1 mL aqueous solution containing ***cis*-O'O@NPs**, ***cis*-O'S@NPs**, ***cis*-S'S@NPs**, ***trans*-O'O@NPs**, ***trans*-O'S@NPs**, or ***trans*-S'S@NPs**. The solution was irradiated with Xe light (640 nm, 2.5 mW/cm^2) for different time intervals (0-30 min). The fluorescence spectrum of the solution was acquired in the range of 500-550 nm with the excitation wavelength of 488 nm. Methylene blue (**MB**) was used as the reference standard (Φ_{Δ} = 0.50 in H_2O)[4] and studied under the same experimental conditions (640 nm, 2.5 mW/cm^2). The absorbance of samples at the irradiation wavelength was set to be ~ 0.1. The singlet oxygen quantum yields were calculated by comparing the slopes of SOSG emission increase at 525 nm.

Total ROS detection

ROS generation in live cells was determined using 2',7'-dichlorodihydrofluorescein diacetate (DCFH-DA), an indicator that reacts with cellular ROS to provide an increase in green fluorescence (DCF).[5] HeLa cells were seeded into confocal dishes. ***cis*-O'S@NPs** or ***cis*-S'S@NPs** (0.1 μM) was then added. After 24 hours, DCFH-DA (10 μM) was added and incubated for another 30 mins. The cells treated with different conditions (***cis*-O'S@NPs**, ***cis*-O'S@NPs** + $h\upsilon$, ***cis*-S'S@NPs**, and ***cis*-S'S@NPs** + $h\upsilon$) were then imaged under a confocal fluorescence microscopy (Ex 488 / Em 525).

Cell culture and cytotoxicity assay

HeLa cells were cultured in Dulbecco's modified Eagle medium (DMEM, Corning) supplemented with 10% fetal bovine serum (FBS), 1% penicillin and streptomycin in an atmosphere of 5% CO_2 and 95% air at 37 °C.

HeLa cells were seeded into 96-well plates (10^4 cells per well) for 24 hours. The cells were incubated with ***cis*-O'S@NPs** or ***cis*-S'S@NPs** at different concentrations (0-10 μM) for 24 hours. The cell viability was measured using the Cell Counting Kit-8 (CCK-8) assay. 100 μL fresh medium containing 10% Cell Counting Kit-8 (CCK-8) was added to each well followed by incubation for 1 h. The absorbance at 450 nm was measured using a Microplate Reader. The viability of HeLa cells was calculated using the following equation:

$$CV = (A - A_0) / (A_c - A_0) \times 100\%$$

where CV = cell viability, A, A_c and A_0 represent the absorbance of cells incubated with ***cis*-O'S@NPs** or ***cis*-S'S@NPs**, control group, and background group, respectively.

After incubated with different concentrations (0-10 μM) of ***cis*-O'S@NPs** and ***cis*-S'S@NPs** for 24 hours, the cells were washed with PBS and then irradiated with LED light (700 nm, 2.5 mW/cm^2) for 10 mins. The cell viability was determined using the CCK-8 assay.

Calcein-AM/PI assay

To visually demonstrate the cytotoxicity of ***cis*-O'S@NPs** and ***cis*-S'S@NPs**, HeLa cells were incubated with ***cis*-O'S@NPs** or ***cis*-S'S@NPs** (0.1 μM) at 37 °C for 24 hours and then co-stained with 2 μM Calcein-AM (for live cells) and 4 μM PI (for dead cells) for 10 mins. The cells treated with different conditions (***cis*-O'S@NPs**, ***cis*-O'S@NPs** + $h\upsilon$, ***cis*-S'S@NPs**, and ***cis*-S'S@NPs** + $h\upsilon$) were imaged under a confocal fluorescence microscopy.

3D multicellular spheroids (MCSs)

HeLa cells were seeded in a 96-well plate to form MCSs with diameters of about 500 μm. The HeLa MCSs were divided into different groups and cultured in media containing ***cis*-O'S@NPs** and ***cis*-S'S@NPs** (6 μM) for 24 hours, respectively. Then the medium was refreshed. The light groups were irradiated with a 700 nm LED lamp (10 mW/cm^2) for 10 min. Images were recorded on a microscope every day.

***In vivo* experiments**

All animal procedures were approved by the Institutional Animal Care and Use Committee of Sinoresearch (Beijing) Biotechnology Co., Ltd. (protocol number: ZYZC202306011J). Five weeks old BALB/c nude mice were inoculated with HeLa cells (5

$\times 10^6$ cells per mice) to establish the tumor model used in the present study. When the tumor volume reached approximately 100 mm^3, the mice were randomly divided into five groups (n = 4) and intravenously injected with ***cis*-O'S@NPs/*cis*-S'S@NPs** (2 mg/kg), or PBS (200 μL) respectively. The tumors in different mice groups ("Control (PBS + $h\upsilon$)", "***cis*-O'S @NPs**", "***cis*-S'S@NPs**", "***cis*-O'S@NPs** + $h\upsilon$", and "***cis*-S'S@NPs** + $h\upsilon$") were subject to photoirradiation for 10 mins using LED light sources (700 nm, 200 mW/cm^2). The tumor size and body weight of each mouse were measured every two days. After 14 days, the mice were sacrificed and the tumors were sectioned. Hematoxylin and eosin (H&E) staining analyses of the main organs (heart, liver, spleen, lung and kidney) were also carried out.

Statistical analysis

Data are presented as mean ± SD. Dunnett's t-tests were used to determine whether the variance between two groups is similar. One-way ANOVA was applied for comparison of multiple groups. Statistical analysis was performed using GraphPad Prism. $P < 0.05$ was considered statistically significant.[6]

Theoretical and computational details

Geometry optimizations for ground (S_0) and excited states (S_1, T_1, and T_2) followed by harmonic vibrational frequencies calculation with hybrid density functional, B3LYP[7] with "D3BJ" dispersion corrections, were performed using the program package Gaussian 09 (Revision E.01).[8] The 6-311G(d, p) basis set[9] was used for all atoms. Solvent effects (including the geometry optimizations and frequencies) were considered by means of SMD[10] model for dichloromethane match the experimental conditions. Frequency calculations were performed on the optimized structures to ensure that they were minimum energy structures by the absence of imaginary frequency. Stability calculations were also performed for all the optimized structures to ensure that all the wavefunctions obtained were stable.

The spin-orbit coupling (SOC) integrals between the spin state S_n and T_m, $\langle T_m|\hat{H}_{SO}|S_n\rangle$, were estimated using effective atomic charge (Zeff) method by PySOC.[11] The radiative decay rate constant, intersystem crossing rate constant and non-radiative decay rate constant were calculated by MOMAP program package using a thermal vibration correlation function formalism for the transition between two adiabatic electronic states considering

displacements, distortions, and Duschinsky rotation of potential energy surfaces within the framework of multidimensional harmonic oscillator model and Franck-Condon principle.[12]

All the molecular dynamic simulations were performed using the AmberTools 18 software package.[13] The general AMBER force field (GAFF[14]) was used for the *cis*-isomers (***cis*-O'O**, ***cis*-O'S**, ***cis*-S'S**, and ***trans*-O'O**). Water molecules were treated by TIP3P model. A spherical cut-off of 0.7 nm for the summation of van der Waals (VDW) interactions and short-range Coulomb interactions and the particle-mesh Ewald solver for long-range Coulomb interactions were used throughout. The simulations were carried out with three-dimensional periodic boundary conditions using the leap-frog integrator with a time step of 1.0 fs. The molecular dynamics simulation workflow includes five steps: (1) Randomly placing 9 *cis*-isomers and in a water box ($50 \times 50 \times 50$ nm^3) to generate an initial geometry, then followed by 4000 steps minimization. (2) Then the system was heated from 0 to 300 K under a canonical ensemble for 50 ps with a weak restraint of 15 kcal/(mol Å). (3) To achieve a uniform density after heating dynamics, 1 ns of density equilibration was performed under the NPT ensemble at the target temperature of 300 K and target pressure of 1.0 atm. (4) 4 ns of equilibration at 300 K and 1 bar (equilibration). (5) 200 ns of equilibration at 300 K with constant volume (NVT ensemble equilibration). 10000 snapshots were sampled from the MD trajectories every 10 ps in last 100 ns MD simulation to calculate the intermolecular dihedral distribution and the distribution of angle of transition dipole moments according to TD-DFT calculation. The Langevin dynamics with the collision frequency 5.0 were applied to control the temperature.

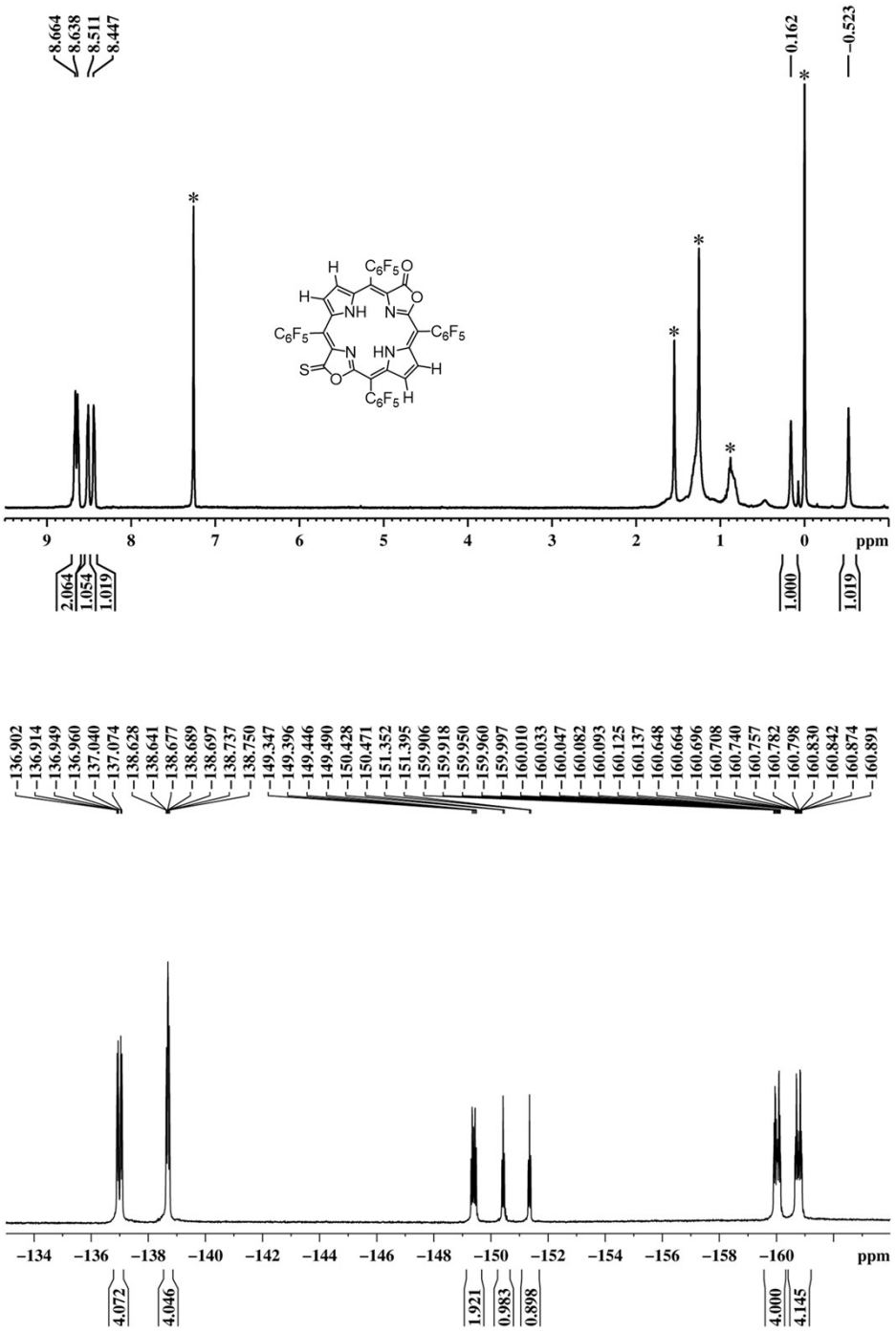

Figure S1. ^{1}H and ^{19}F NMR spectra of ***cis*-O'S** in $CDCl_3$ at 293 K. * indicate the residual solvent and H_2O signals.

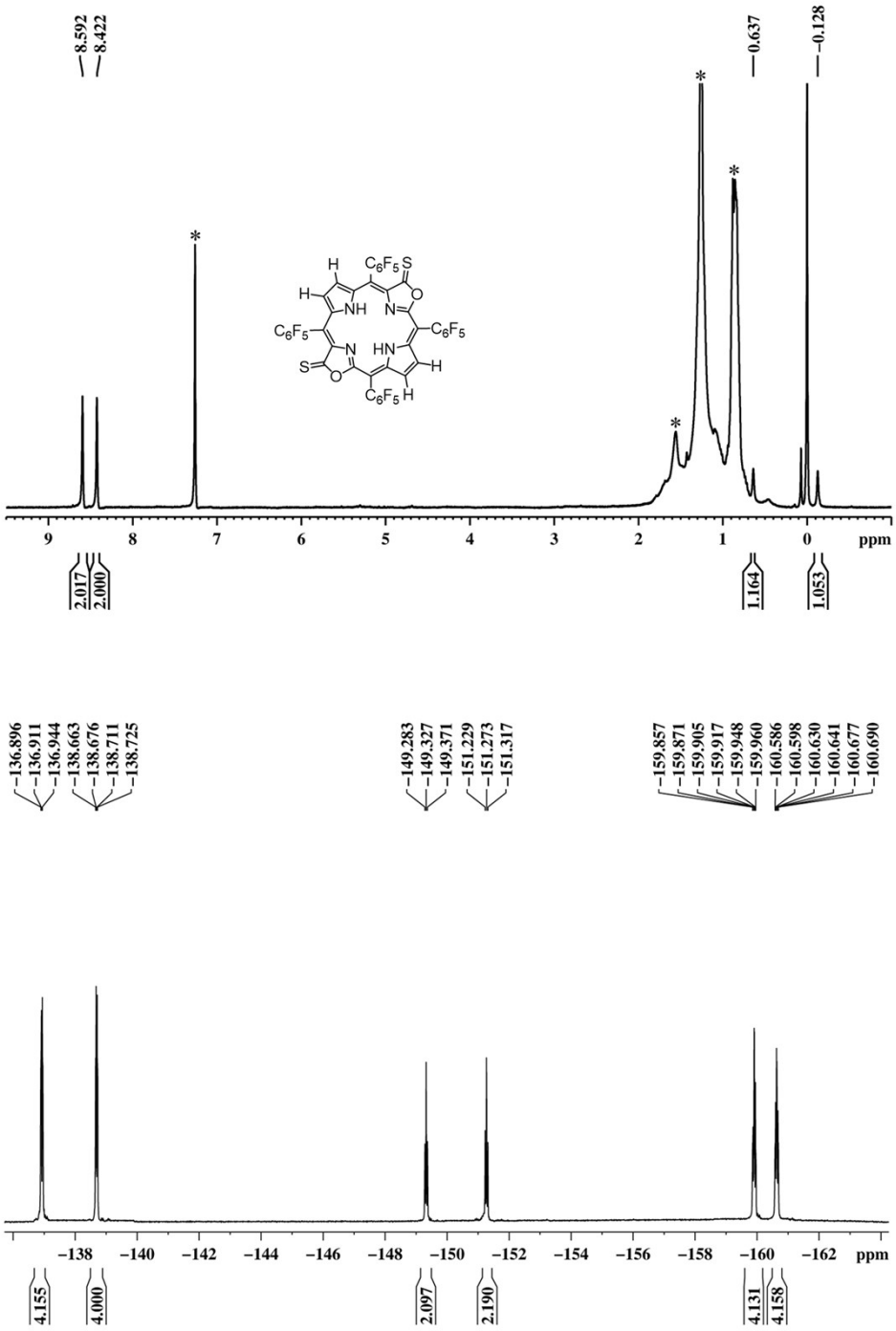

Figure S2. ^{1}H and ^{19}F NMR spectra of ***cis*-S'S** in $CDCl_3$ at 293 K. * indicate the residual solvent and H_2O signals.

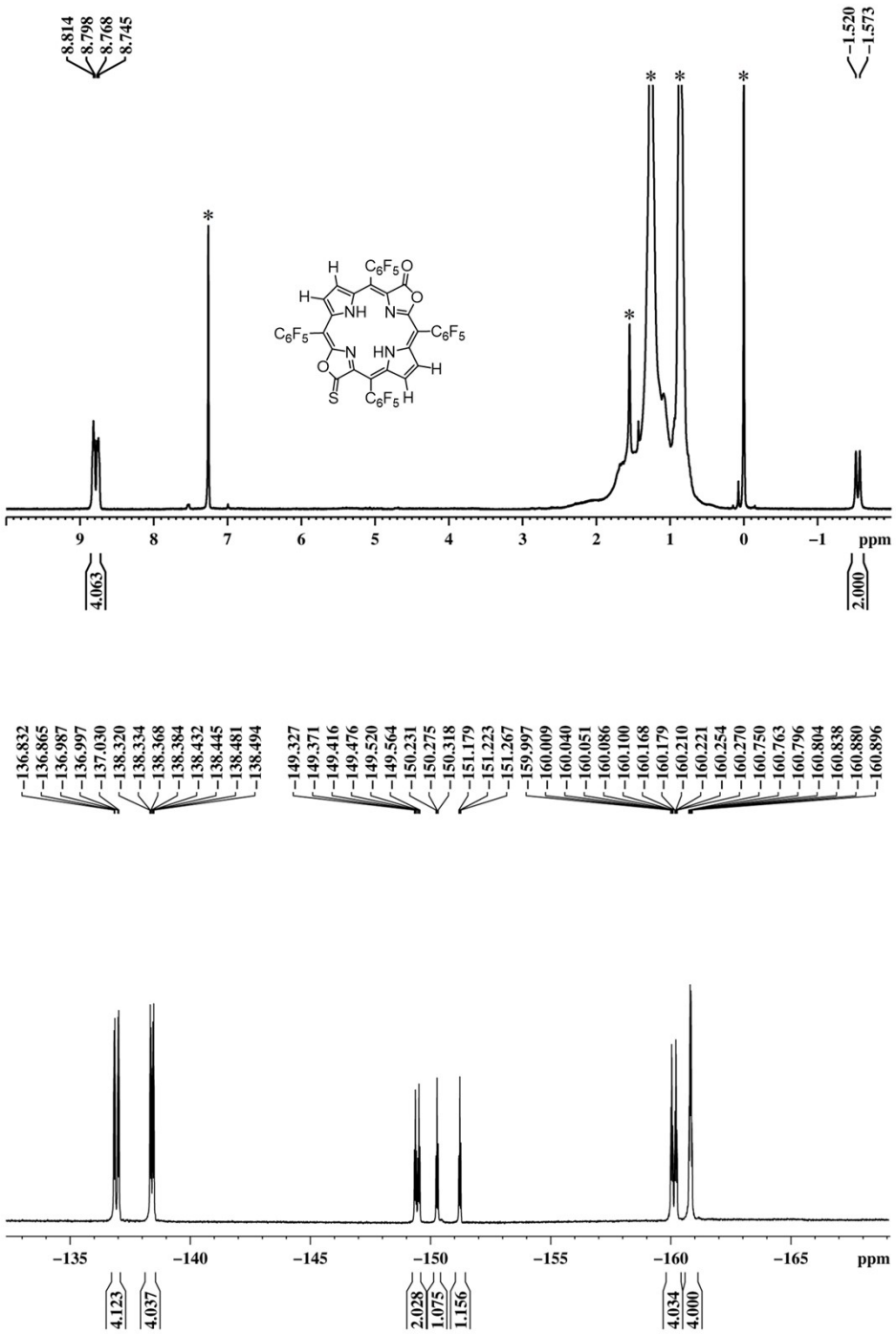

Figure S3. ^{1}H and ^{19}F NMR spectra of ***trans*-O'S** in $CDCl_3$ at 293 K. * indicate the residual solvent and H_2O signals.

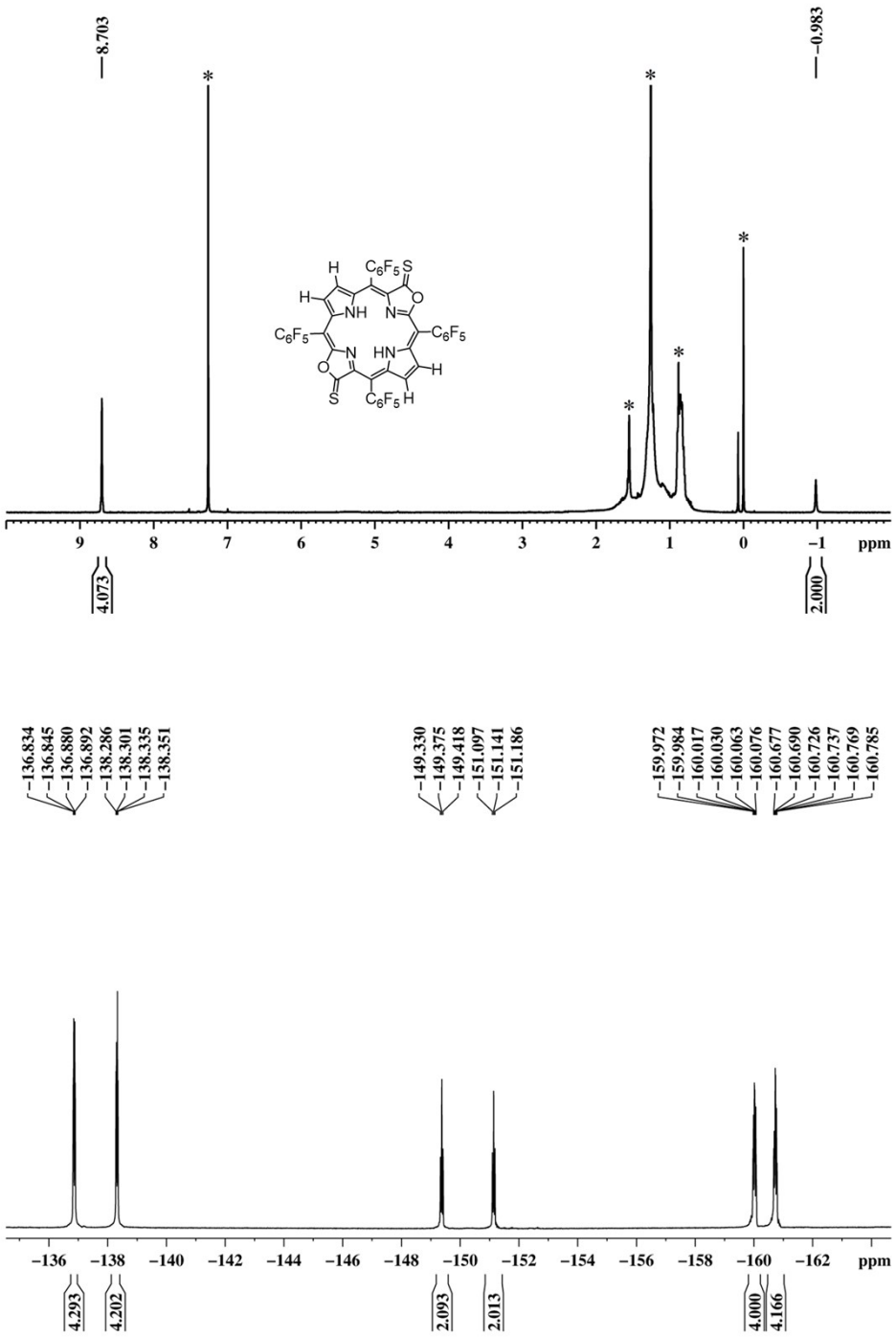

Figure S4. ^{1}H and ^{19}F NMR spectra of ***trans*-S'S** in $CDCl_3$ at 293 K. * indicate the residual solvent and H_2O signals.

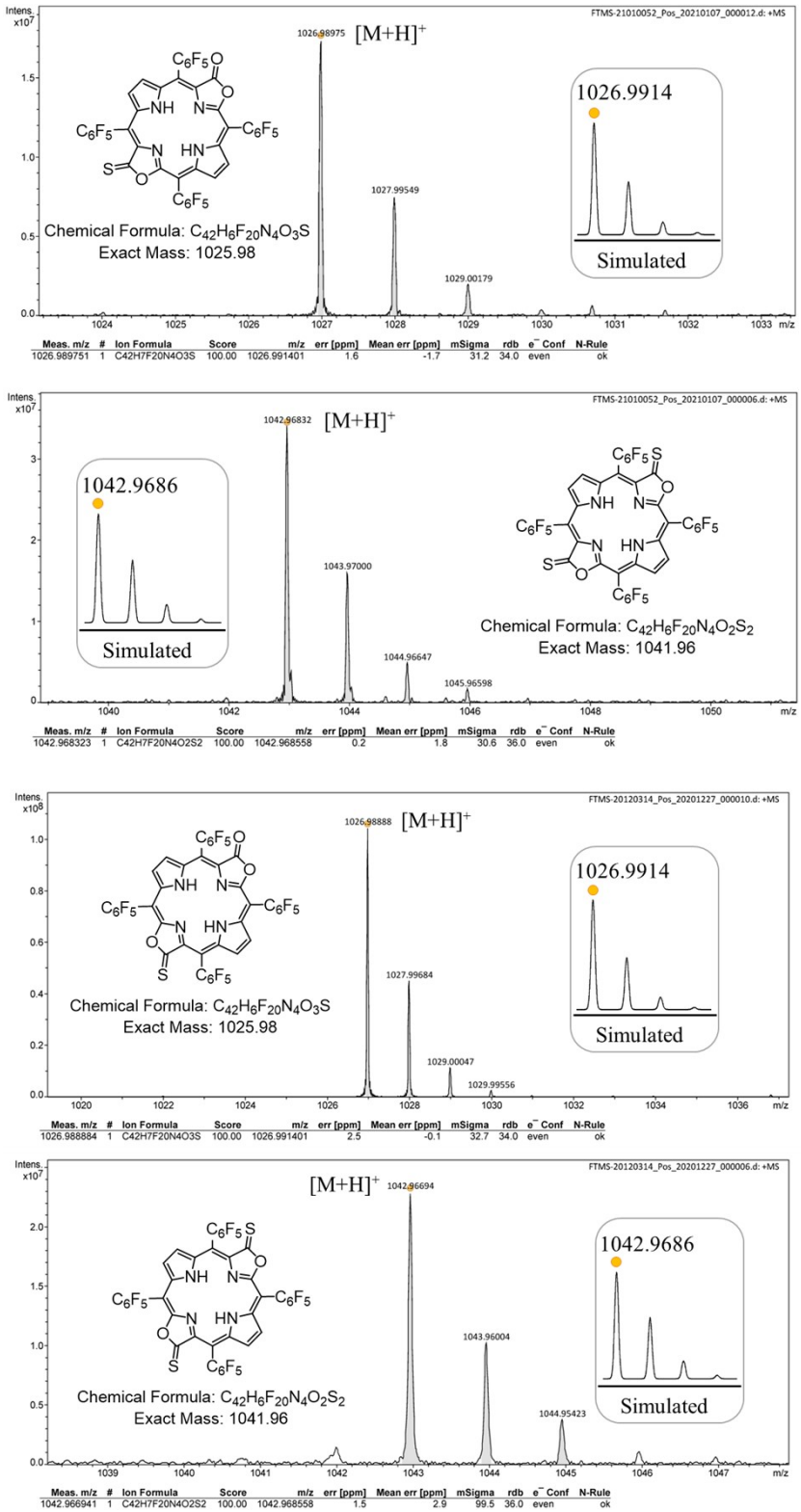

Figure S5. HR-MS spectra of ***cis*-O'S**, ***cis*-S'S**, ***trans*-O'S**, and ***trans*-S'S**.

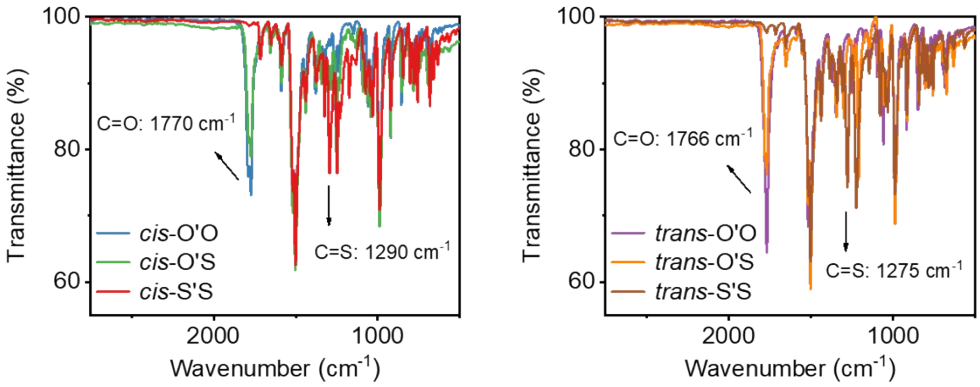

Figure S6. FT-IR spectra of ***cis*-O'O**, ***cis*-O'S**, ***cis*-S'S**, ***trans*-O'O**, ***trans*-O'S**, and ***trans*-S'S**.

Table S1. Crystal data and structure refinement.

Compound	***cis*-O'S** (CCDC: 2261655)	***cis*-S'S** (CCDC: 2261661)	***trans*-O'S** (CCDC: 2261656)	***trans*-S'S** (CCDC: 2261662)
Molecular formula	$C_{42}H_6F_{20}N_4O_3S$	$C_{42}H_6F_{20}N_4O_2S_2$	$C_{42}H_6F_{20}N_4O_3S$	$C_{42}H_6F_{20}N_4O_2S_2$
Formula wt. (g mol^{-1})	1026.56	1042.62	1026.56	1042.62
Temperature (K)	180	180	180	180
Radiation (Å)	0.71073	0.71073	0.71073	0.71073
Crystal system	monoclinic	tetragonal	monoclinic	orthorhombic
Space group	P 21/c	I 4/m	P 21/n	P b c a
a (Å)	12.5483(3)	12.38990(10)	15.4250(6)	11.9737(2)
b (Å)	11.9429(3)	12.38990(10)	7.9625(3)	16.1898(3)
c (Å)	15.1906(5)	27.3100(4)	17.8492(8)	22.2877(3)
α (º)	90	90	90	90
β (º)	102.609(3)	90	109.055(4)	90
γ (º)	90	90	90	90
Volume	2221.61(11)	4192.35(9)	2072.14(15)	4320.51(12)
Z	2	4	2	4
ρ_{calcd} (g cm^{-3})	1.535	1.652	1.645	1.729
μ (mm^{-1})	0.200	0.260	0.215	0.260
F (000)	1012	2056	1012	2232
Theta range	2.562 to 25.027	2.325 to 31.321	1.519 to 30.514	1.827 to 30.687
Reflections collected	52166	57509	14989	52873
Independent reflections	3910 [R(int) = 0.0470]	3293 [R(int) = 0.0264]	5435 [R(int) = 0.0305]	6198 [R(int) = 0.0237]
Goodness-of-fit on F^2	1.099	1.033	1.032	1.034
Final R indices [R > 2σ (I)]	R_1 = 0.1000, wR_2 = 0.2434	R_1 = 0.0502, wR_2 = 0.1405	R_1 = 0.0534, wR_2 = 0.1191	R_1 = 0.0498, wR_2 = 0.1439
R indices (all data)	R_1 = 0.1059, wR_2 = 0.2471	R_1 = 0.0562, wR_2 = 0.1445	R_1 = 0.0845, wR_2 = 0.1299	R_1 = 0.0622, wR_2 = 0.1520
Largest diff. peak and hole (e $Å^{-3}$)	0.922 and -0.786	0.472 and -0.604	0.237 and -0.301	0.958 and -0.794

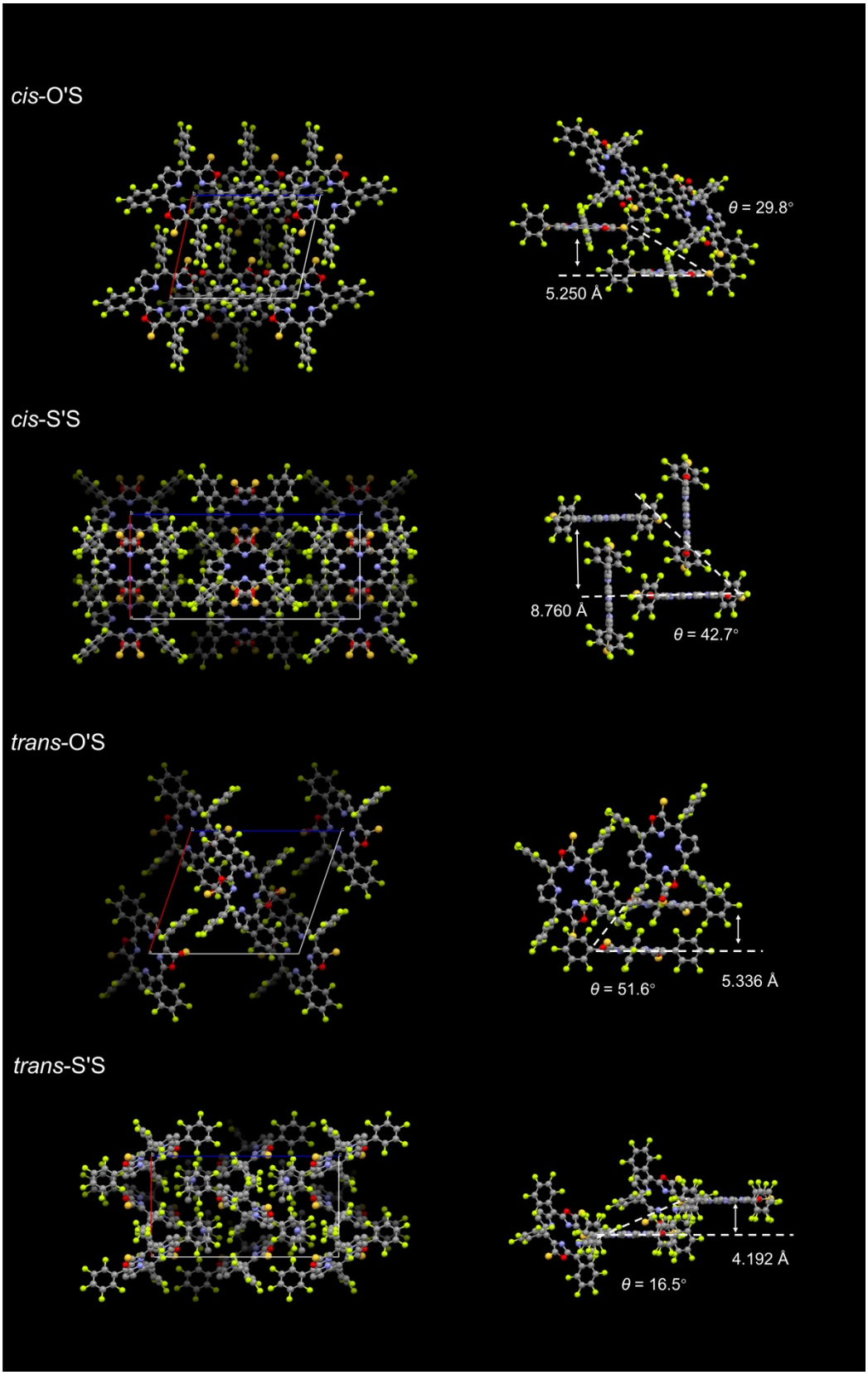

Figure S7. Molecular packing of ***cis*-O'S**, ***cis*-S'S**, ***trans*-O'S**, and ***trans*-S'S** in the single crystal unit cells.

Table S2. Photophysical properties of ***cis*-O'O**, ***cis*-O'S**, ***cis*-S'S**, ***trans*-O'O**, ***trans*-O'S**, and ***trans*-S'S** in CH_2Cl_2.

Compound	Absorption λ_{max} [nm] (Log ε [M^{-1} cm^{-1}])						Emission λ_{max}[a] [nm]	Φ_{em}[b] %	Φ_{Δ}[c] %
***cis*-O'O**	391 (5.10)	408 (5.58)	504 (4.33)	540 (3.85)	600 (4.05)	656 (4.49)	664	15	53
***cis*-O'S**	414 (5.22)	438 (5.57)	545 (4.30)	580 (4.70)	626 (4.12)	692 (4.40)	705	< 0.1	79
***cis*-S'S**		450 (5.55)	580 (4.52)	623 (5.03)	654 (4.41)	720 (4.32)	738	< 0.1	81
***trans*-O'O**		410 (5.54)	511 (4.08)	552 (4.32)	618 (3.91)	676 (4.85)	679	15	60
***trans*-O'S**	424 (5.43)	444 (5.48)	548 (4.18)	588 (4.77)	644 (4.18)	708 (4.84)	722	< 0.1	81
***trans*-S'S**	436 (5.47)	461 (5.44)	581 (4.48)	628 (4.91)	662 (4.44)	734 (4.75)	750	< 0.1	82

[a] Excitation at 405 nm.

[b] Fluorescence quantum yields were determined referenced to **TPP** in CH_2Cl_2 (Φ_{em} = 11%).[2]

[c] Singlet oxygen quantum yields of were determined referenced to **TPP** in $CHCl_3$ (Φ_{Δ} = 55%).[3]

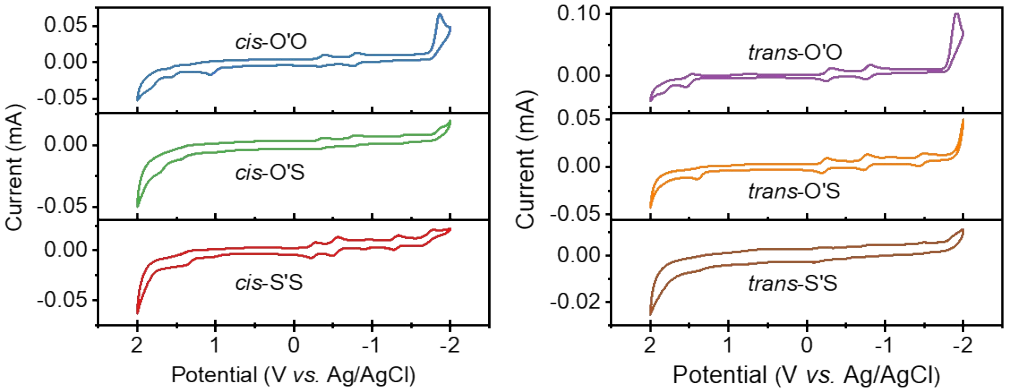

Figure S8. Cyclic voltammograms of ***cis*-O'O**, ***cis*-O'S**, ***cis*-S'S**, ***trans*-O'O**, ***trans*-O'S**, and ***trans*-S'S** in CH_3CN.

Table S3. CV data for ***cis*-O'O**, ***cis*-O'S**, ***cis*-S'S**, ***trans*-O'O**, ***trans*-O'S**, and ***trans*-S'S** in CH_3CN.[a]

Compound	Oxidation [V]	Reduction [V]				HOMO-LUMO gap[b]
	E_{ox1}	E_{red1}	E_{red2}	E_{red3}	E_{red4}	[eV]
***cis*-O'O**	+1.53	-0.36	-0.78			1.89
***cis*-O'S**	+1.39	-0.35	-0.76	-1.42		1.74
***cis*-S'S**	+1.33	-0.25	-0.52	-0.92	-1.30	1.58
***trans*-O'O**	+1.49	-0.29	-0.78			1.78
***trans*-O'S**	+1.37	-0.22	-0.75	-1.47		1.59
***trans*-S'S**	+1.32	-0.15	-0.49	-0.76	-1.46	1.47

[a] Cyclic voltammetry (CV) in nitrogen-saturated CH_3CN containing a 0.10 M NBu_4PF_6 supporting electrolyte. A Pt counter electrode, a 3 mm diameter glassy carbon working electrode, and an Ag/AgCl reference electrode were used. Scan rate: 100 $mV \cdot s^{-1}$. T = 20 °C.

[b] The potential difference between the first oxidation and first reduction.

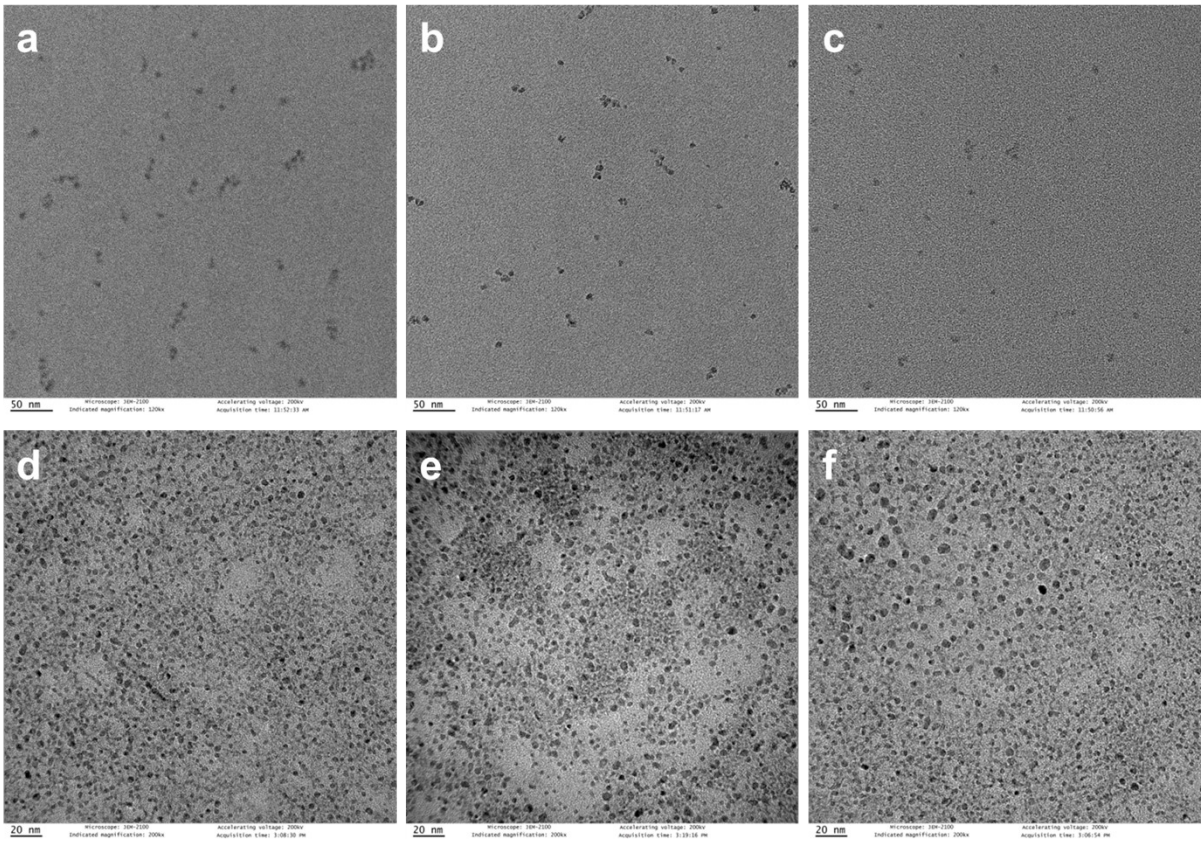

Figure S9. TEM images of ***cis*-O'O@NPs** (a), ***cis*-O'S@NPs** (b), ***cis*-S'S@NPs** (c), ***trans*-O'O@NPs** (d), ***trans*-O'S@NPs** (e), and ***trans*-S'S@NPs** (f).

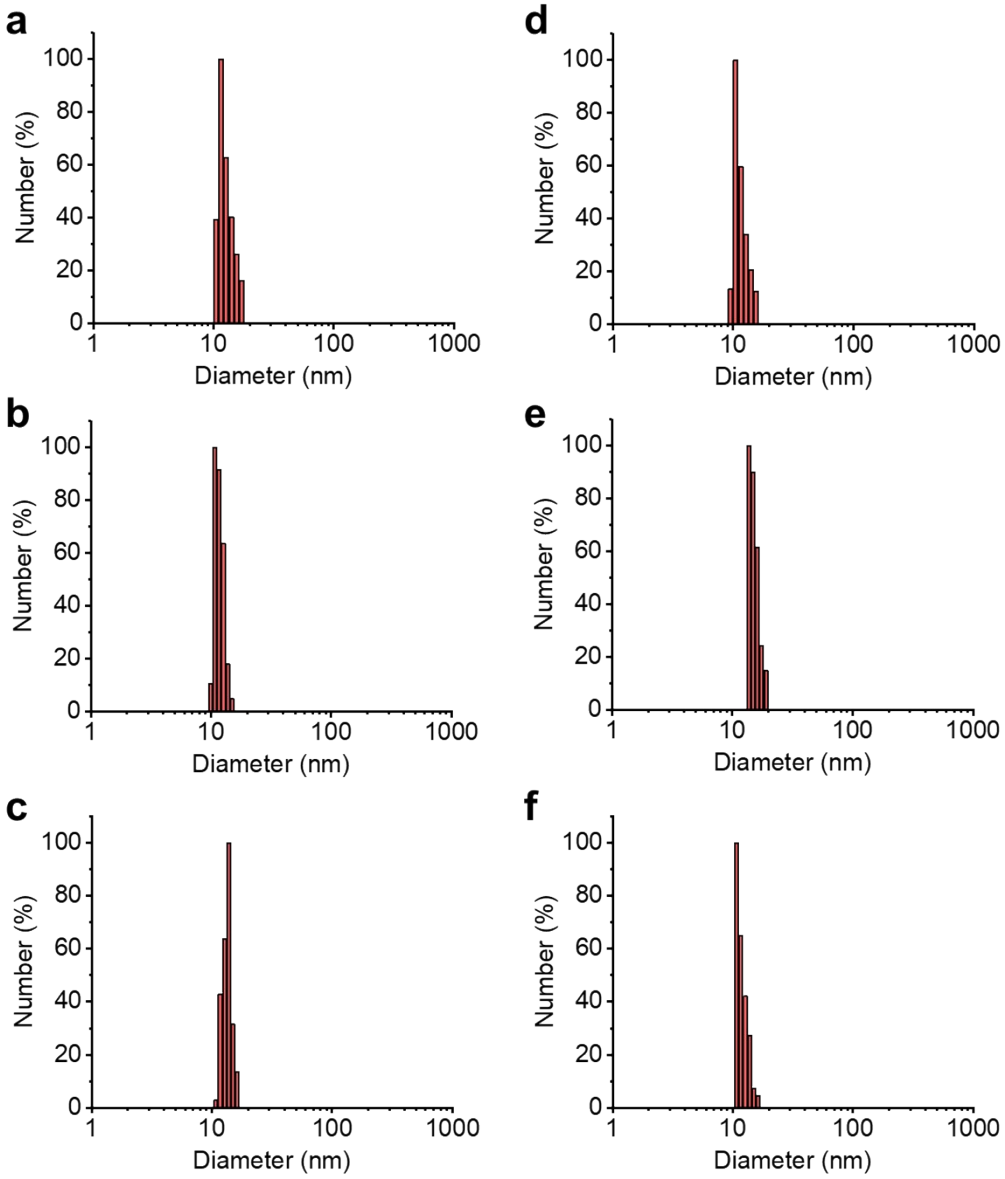

Figure S10. Size distributions of ***cis*-O'O@NPs** (a), ***cis*-O'S@NPs** (b), ***cis*-S'S@NPs** (c), ***trans*-O'O@NPs** (d), ***trans*-O'S@NPs** (e), and ***trans*-S'S@NPs** (f) obtained by DLS.

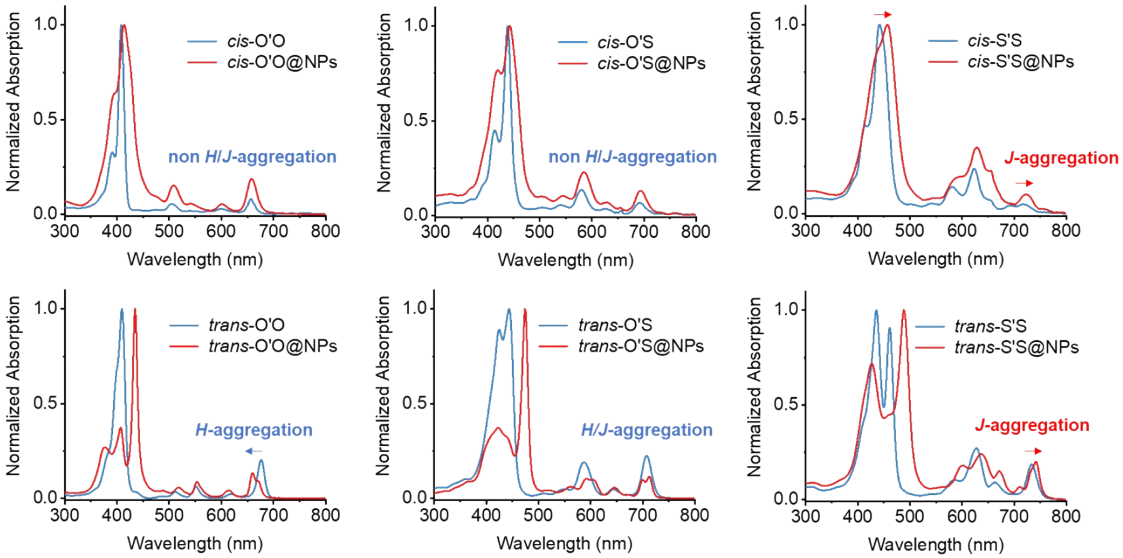

Figure S11. Normalized absorption spectra of ***cis*-O'O**, ***cis*-O'S**, ***cis*-S'S**, ***trans*-O'O**, ***trans*-O'S**, and ***trans*-S'S** in CH_2Cl_2 and normalized absorption spectra of ***cis*-O'O@NPs**, ***cis*-O'S@NPs**, ***cis*-S'S@NPs**, ***trans*-O'O@NPs**, ***trans*-O'S@NPs**, and ***trans*-S'S@NPs** in aqueous solution.

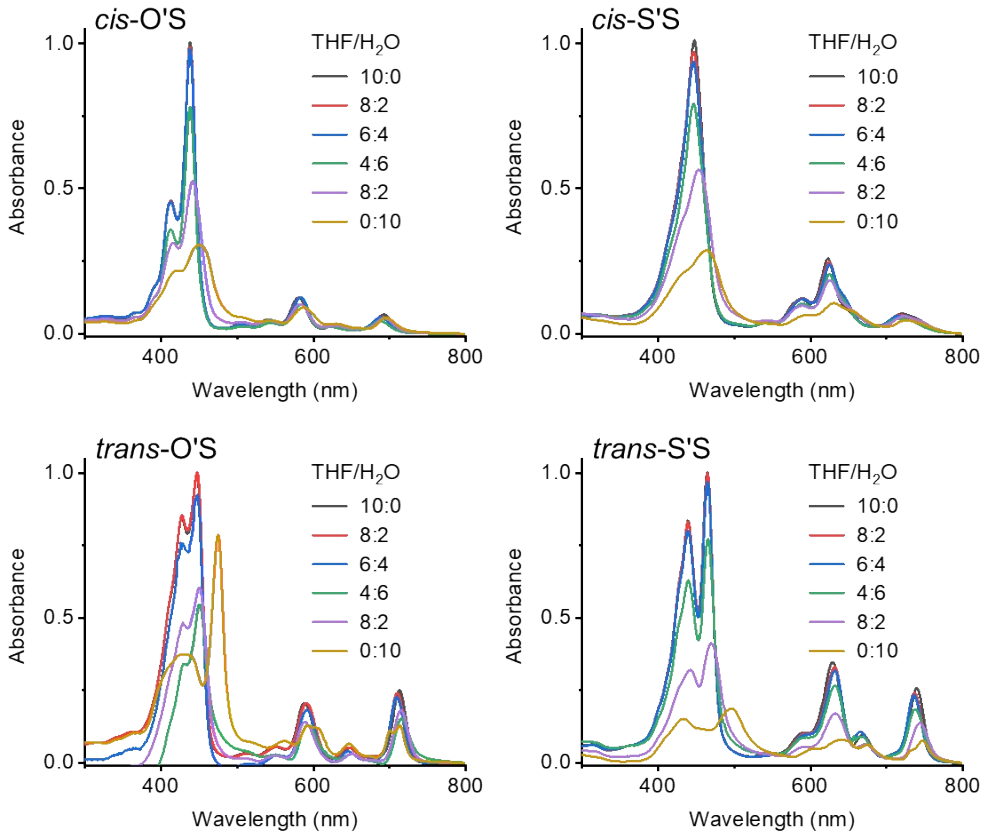

Figure S12. Absorption spectra of ***cis*-O'S**, ***cis*-S'S**, ***trans*-O'S**, and ***trans*-S'S** in THF-H_2O mixed solvents with varying ratios (v/v).

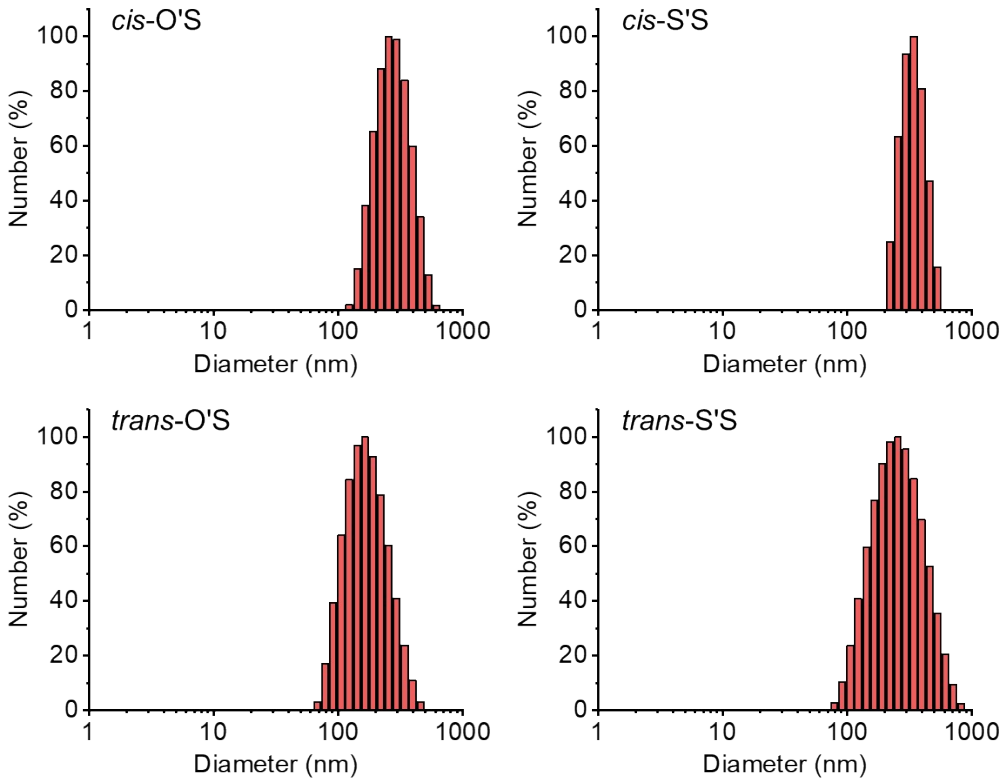

Figure S13. Size distributions of ***cis*-O'S**, ***cis*-S'S**, ***trans*-O'S**, and ***trans*-S'S** in H_2O obtained by DLS.

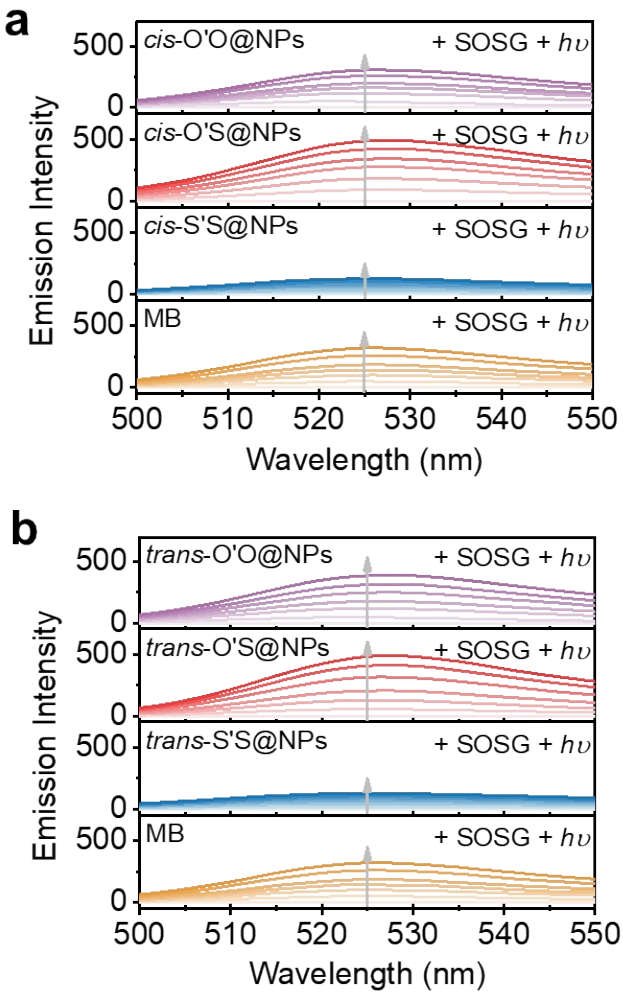

Figure S14. (a) Fluorescence spectra of SOSG (5 μM, λ_{ex} = 488 nm) in H_2O under light irradiation (0-30 min) in the presence of ***cis*-O'O@NPs**, ***cis*-O'S@NPs**, ***cis*-S'S@NPs**, and MB. (b) Fluorescence spectra of SOSG (5 μM, λ_{ex} = 488 nm) in H_2O under light irradiation (0-30 min) in the presence of ***trans*-O'O@NPs**, ***trans*-O'S@NPs**, ***trans*-S'S@NPs**, and MB.

Table S4. Photophysical properties of ***cis*-O'O@NPs**, ***cis*-O'S@NPs**, ***cis*-S'S@NPs**, ***trans*-O'O@NPs**, ***trans*-O'S@NPs**, and ***trans*-S'S@NPs** in H_2O.

Compound	Absorption λ_{max} [nm]						Emission λ_{max}[a] [nm]	Φ_Δ[b] %	η[c] %
***cis*-O'O@NPs**	395	414	509	542	601	658	--	48	55
***cis*-O'S@NPs**	420	443	544	585	628	695	--	78	18
***cis*-S'S@NPs**		457	586	629	656	722	--	20	23
***trans*-O'O@NPs**	376/407	435	518	553	615	659	--	62	40
***trans*-O'S@NPs**	423	474	562	591/608	646	700/712	--	81	20
***trans*-S'S@NPs**	427	488	600	638	672	742	--	21	26

[a] Not determined.

[b] Singlet oxygen quantum yields of were determined referenced to **MB** in H_2O (Φ_Δ = 50%).

[c] Photothermal conversion efficiency in water.

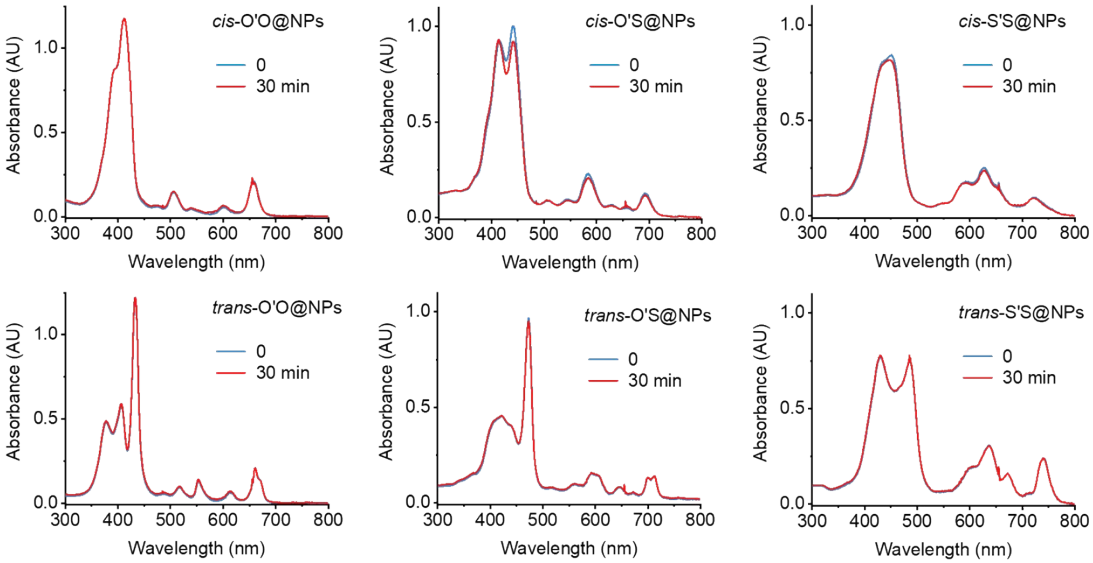

Figure S15. The absorption spectra of ***cis*-O'O@NPs**, ***cis*-O'S@NPs**, ***cis*-S'S@NPs**, ***trans*-O'O@NPs**, ***trans*-O'S@NPs**, and ***trans*-S'S@NPs** in aqueous solution recorded before and after continuous photoirradiation (700 nm, 5 mW/cm^2, 30 min).

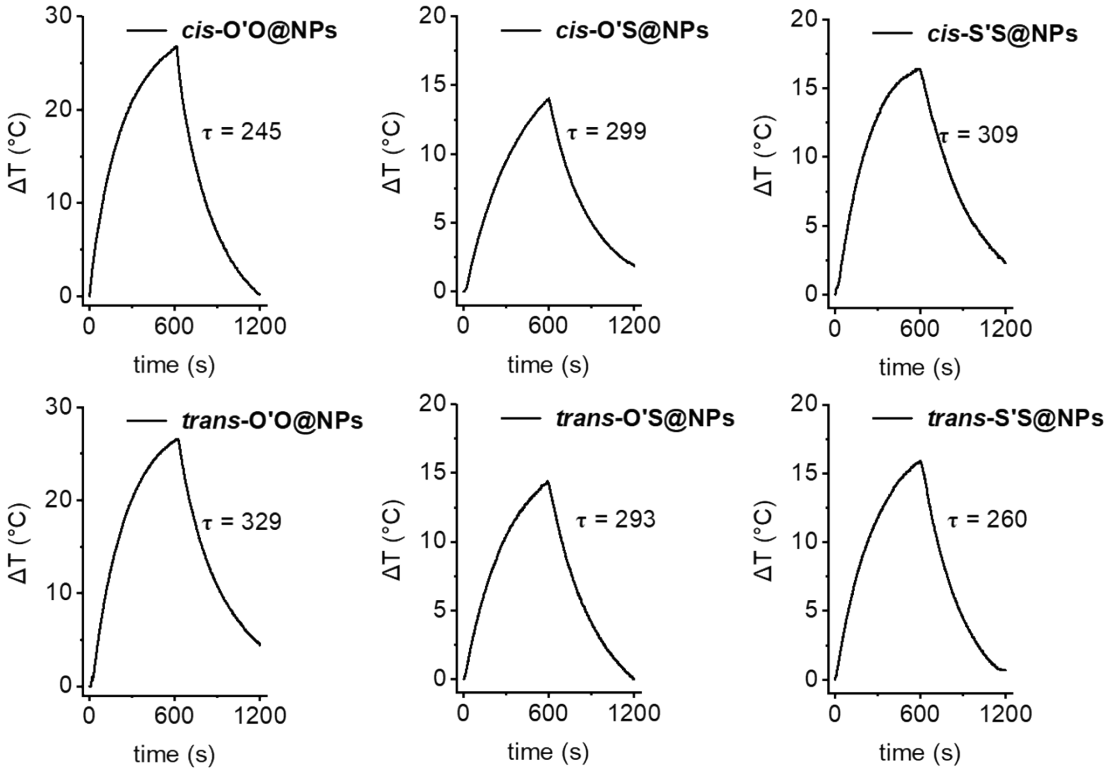

Figure S16. Photothermal effect of ***cis*-O'O@NPs**, ***cis*-O'S@NPs**, ***cis*-S'S@NPs**, ***trans*-O'O@NPs**, ***trans*-O'S@NPs**, and ***trans*-S'S@NPs** in aqueous solution upon photoirradiation with a 650 nm laser (A = 0.5, 1 W/cm^2).

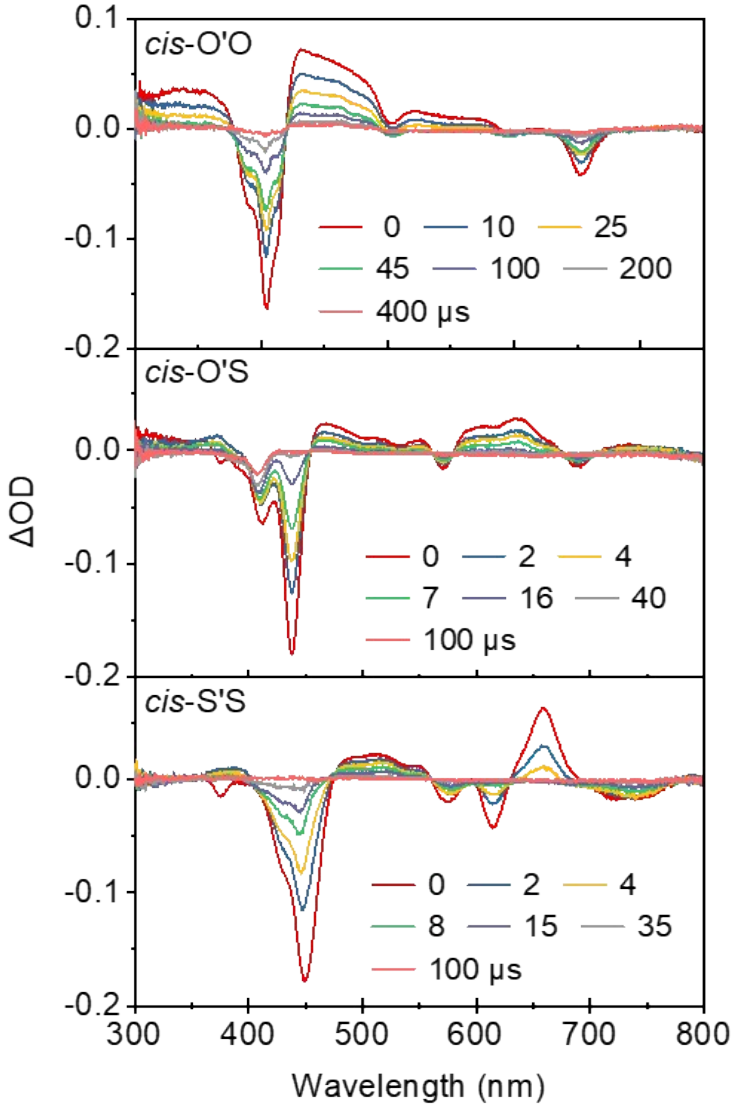

Figure S17. ns-TA difference spectra for ***cis*-O'O**, ***cis*-O'S**, and ***cis*-S'S** recorded at selected decay times in degassed CH_2Cl_2.

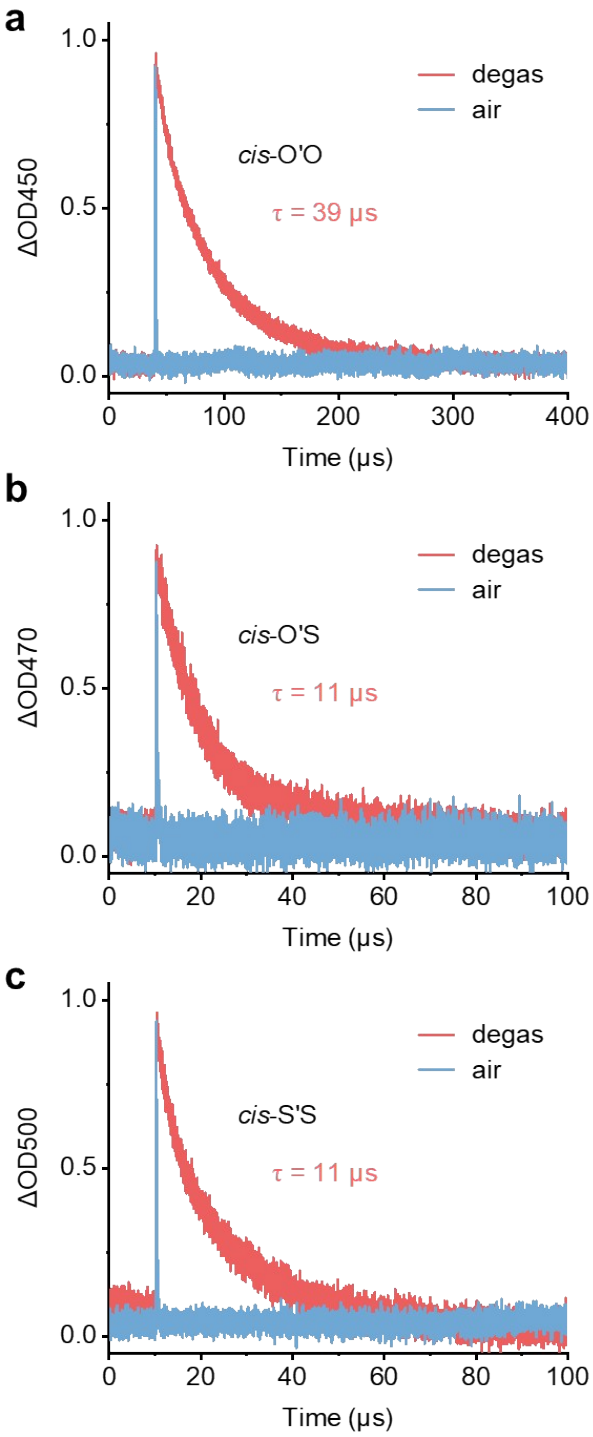

Figure S18. The ESA kinetic decay traces of ***cis*-O'O** (a), ***cis*-O'S** (b), and ***cis*-S'S** (c) recorded under degassed (red) and aerobic conditions (blue), respectively.

Table S5. Summary of the key lifetimes of ***cis*-O'O**, ***cis*-O'S**, ***cis*-S'S**, as well as ***cis*-O'O@NPs**, ***cis*-O'S@NPs**, ***cis*-S'S@NPs** considered in fs-TA study.

	τ ($S_1 \rightarrow S_0$) [a]	k ($S_1 \rightarrow T_0$)	τ ($S_1 \rightarrow T_1$)	k ($S_1 \rightarrow T_1$) [f]	τ ($T_1 \rightarrow S_0$)	k ($T_1 \rightarrow S_0$) [j]
***cis*-O'O**	3714 ps ($R^2 = 0.999$)	2.7×10^8 s^{-1} [b]	--	--	--	--
***cis*-O'O@NPs**	289.1 ps ($R^2 = 0.993$)	3.5×10^9 s^{-1} [c]	--	--	--	--
***cis*-O'S**	--	--	27.10 ps [d] ($R^2 = 0.996$)	3.7×10^{10} s^{-1}	6946 ps [g] ($R^2 = 0.999$)	1.4×10^8 s^{-1}
***cis*-O'S@NPs**	--	--	29.21 ps [d] ($R^2 = 0.992$)	3.4×10^{10} s^{-1}	5275 ps [g] ($R^2 = 0.938$)	1.9×10^8 s^{-1}
***cis*-S'S**	--	--	25.89 ps [e] ($R^2 = 0.998$)	3.9×10^{10} s^{-1}	5612 ps [h] ($R^2 = 0.998$)	1.8×10^8 s^{-1}
***cis*-S'S@NPs**	--	--	24.65 ps [e] ($R^2 = 0.995$)	4.1×10^{10} s^{-1}	-- [i]	-- [i]

[a] Decay traces fitting of 665 nm. [b] Rate constant of radiative relaxation. [c] Rate constant of nonradiative relaxation. [d] Growth traces fitting of 650 nm. [e] Growth traces fitting of 665nm. [f] Rate constant of ISC. [g] Decay traces fitting of 700 nm. [h] Decay traces fitting of 665 nm. [i] No convergence of fitting. [j] Rate constant of triplet decay.

Table S6. Adiabatic energy difference, reorganization energy spin-orbit coupling matrix elements and photophysical rate constants for ***cis*-O'O**, ***cis*-O'S** and ***cis*-S'S** as inferred from DFT calculations.

Compound	***cis*-O'O**						
	$S_1 \rightarrow S_0$	$S_1 \rightarrow T_1$	$S_1 \rightarrow T_2$	$S_1 \rightarrow T_3$			
ΔE_{ST} [eV][a]	2.03	0.78	0.59	0.25			
λ [cm^{-1}][b]	298.8 345.3	188944 187306	607.9 655.7	449 531			
$\langle T_m \lvert \hat{H}_{SO} \rvert S_n \rangle$ [cm^{-1}][c]	--	1.10	0.03	0.27			
k_R [s^{-1}] ($S_1 \rightarrow S_0$)[d]	4.99×10^7	--	--	--			
k_{NR} [s^{-1}] ($S_1 \rightarrow S_0$)[e]	1.34×10^5	--	--	--			
k_{ISC} [s^{-1}] ($S_1 \rightarrow T_n$)[f]	--	--	5.83×10^3	5.03×10^6			
Compound	***cis*-O'S**						
	$S_1 \rightarrow S_0$	$S_1 \rightarrow T_1$	$S_1 \rightarrow T_2$	$S_1 \rightarrow T_3$	$S_1 \rightarrow T_4$	$S_1 \rightarrow T_5$	
ΔE_{ST} [eV][a]	1.94	0.65	0.53	0.30	0.22	0--	
λ [cm^{-1}][b]	328.8 383.4	1717 1813	262 411	384 339	11286 10483	152701 157459	
$\langle T_m \lvert \hat{H}_{SO} \rvert S_n \rangle$ [cm^{-1}][c]		2.29	2.70	0.24	0.27	11.88	
k_R [s^{-1}] ($S_1 \rightarrow S_0$)[d]	3.01×10^7	--	--	--	--	--	
k_{NR} [s^{-1}] ($S_1 \rightarrow S_0$)[e]	2.45×10^3	--	--	--	--	--	
k_{ISC} [s^{-1}] ($S_1 \rightarrow T_n$)[f]	--	4.63×10^8	1.08×10^6	3.41×10^6	1.12×10^6	--	
Compound	***cis*-S'S**						
	$S_1 \rightarrow S_0$	$S_1 \rightarrow T_1$	$S_1 \rightarrow T_2$	$S_1 \rightarrow T_3$	$S_1 \rightarrow T_4$	$S_1 \rightarrow T_5$	$S_1 \rightarrow T_6$
ΔE_{ST} [eV][a]	1.91	0.80	0.51	0.33	0.31	0.28	0.21
λ [cm^{-1}][b]	488 497	242 253	1558 1701	11969 12074	1432 2920	3803 3533	10946 10537
$\langle T_m \lvert \hat{H}_{SO} \rvert S_n \rangle$ [cm^{-1}][c]	--	37.12	2.08	3.41	2.84	3.30	2.24
k_R [s^{-1}] ($S_1 \rightarrow S_0$)[d]	1.09×10^7	--	--	--	--	--	--
k_{NR} [s^{-1}] ($S_1 \rightarrow S_0$)[e]	9.69×10^6	--	--	--	--	--	--
k_{ISC} [s^{-1}] ($S_1 \rightarrow T_n$)[f]	--	7.33×10^8	3.06×10^8	1.31×10^8	8.75×10^8	5.34×10^8	1.43×10^7

[a] Adiabatic energy difference between the S_1 and T_1 state. [b] Total reorganization energy of S_1 state. [c] Spin-orbit coupling matrix element between the S_1 and T_1 state. [d] Fluorescent rate constant corresponding to the depopulation of the S_1 state. [e] Non-radiative rate constant. [f] Intersystem crossing rate constant corresponding to the conversion from the S_1 state to the corresponding T_n state.

Table S7. Adiabatic energy difference, reorganization energy spin-orbit coupling matrix elements and photophysical rate constants for ***trans*-O'O**, ***trans*-O'S** and ***trans*-S'S** as inferred from DFT calculations.

Compound	***trans*-O'O**					
	$S_1 \rightarrow S_0$	$S_1 \rightarrow T_1$	$S_1 \rightarrow T_2$	$S_1 \rightarrow T_3$		
ΔE_{ST} [eV][a]	1.96	0.71	0.87	0.12		
λ [cm^{-1}][b]	216.3	402	692	406		
$\langle T_m \lvert \hat{H}_{SO} \rvert S_n \rangle$ [cm^{-1}][c]	--	0.64	0.93	0.52		
k_R [s^{-1}] ($S_1 \rightarrow S_0$)[d]	4.49×10^7	--	--	--		
k_{NR} [s^{-1}] ($S_1 \rightarrow S_0$)[e]	7.73×10^3	--	--	--		
k_{ISC} [s^{-1}] ($S_1 \rightarrow T_n$)[f]	--	6.30×10^5	1.10×10^6	5.96×10^7		
Compound	***trans*-O'S**					
	$S_1 \rightarrow S_0$	$S_1 \rightarrow T_1$	$S_1 \rightarrow T_2$	$S_1 \rightarrow T_3$	$S_1 \rightarrow T_4$	
ΔE_{ST} [eV][a]	1.87	0.90	0.90	0.72	0.19	
λ [cm^{-1}][b]	420.6	786.0	189076	447.7	404.7	
$\langle T_m \lvert \hat{H}_{SO} \rvert S_n \rangle$ [cm^{-1}][c]	--	49.91	1.30	0.85	0.94	
k_R [s^{-1}] ($S_1 \rightarrow S_0$)[d]	3.84×10^7	--	--	--	--	
k_{NR} [s^{-1}] ($S_1 \rightarrow S_0$)[e]	9.81×10^4	--	--	--	--	
k_{ISC} [s^{-1}] ($S_1 \rightarrow T_n$)[f]	--	1.26×10^{11}	--	1.05×10^6	1.95×10^8	
Compound	***trans*-S'S**					
	$S_1 \rightarrow S_0$	$S_1 \rightarrow T_1$	$S_1 \rightarrow T_2$	$S_1 \rightarrow T_3$	$S_1 \rightarrow T_4$	$S_1 \rightarrow T_5$
ΔE_{ST} [eV][a]	1.78	0.76	0.45	0.40	0.16	0.16
λ [cm^{-1}][b]	378.8	297.6	3565	1052	240	240
$\langle T_m \lvert \hat{H}_{SO} \rvert S_n \rangle$ [cm^{-1}][c]	--	1.49	71.0	2.15	1.31	0.59
k_R [s^{-1}] ($S_1 \rightarrow S_0$)[d]	3.23×10^7	--	--	--	--	--
k_{NR} [s^{-1}] ($S_1 \rightarrow S_0$)[e]	8.48×10^6	--	--	--	--	--
k_{ISC} [s^{-1}] ($S_1 \rightarrow T_n$)[f]	--	7.94×10^6	5.19×10^{11}	7.90×10^8	2.62×10^8	5.24×10^7

[a] Adiabatic energy difference between the S_1 and T_1 state. [b] Total reorganization energy of S_1 state. [c] Spin-orbit coupling matrix element between the S_1 and T_1 state. [d] Fluorescent rate constant corresponding to the depopulation of the S_1 state. [e] Non-radiative rate constant. [f] Intersystem crossing rate constant corresponding to the conversion from the S_1 state to the corresponding T_n state.

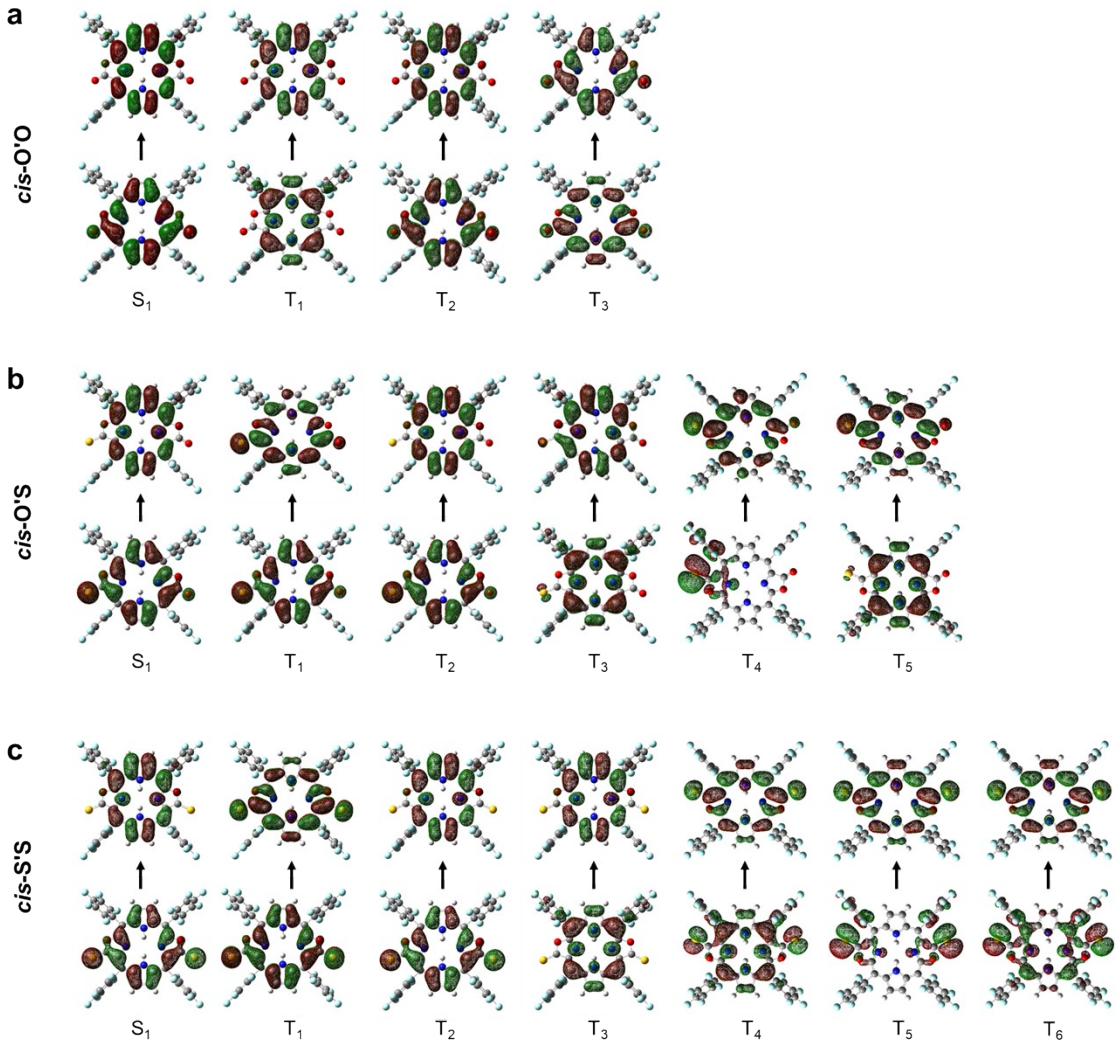

Figure S19. The frontier molecular orbitals of porphodilactone derivatives (***cis*-O'O**, ***cis*-O'S**, and ***cis*-S'S**) in their singlet states (S_1) and triplet states (T_1–T_n).

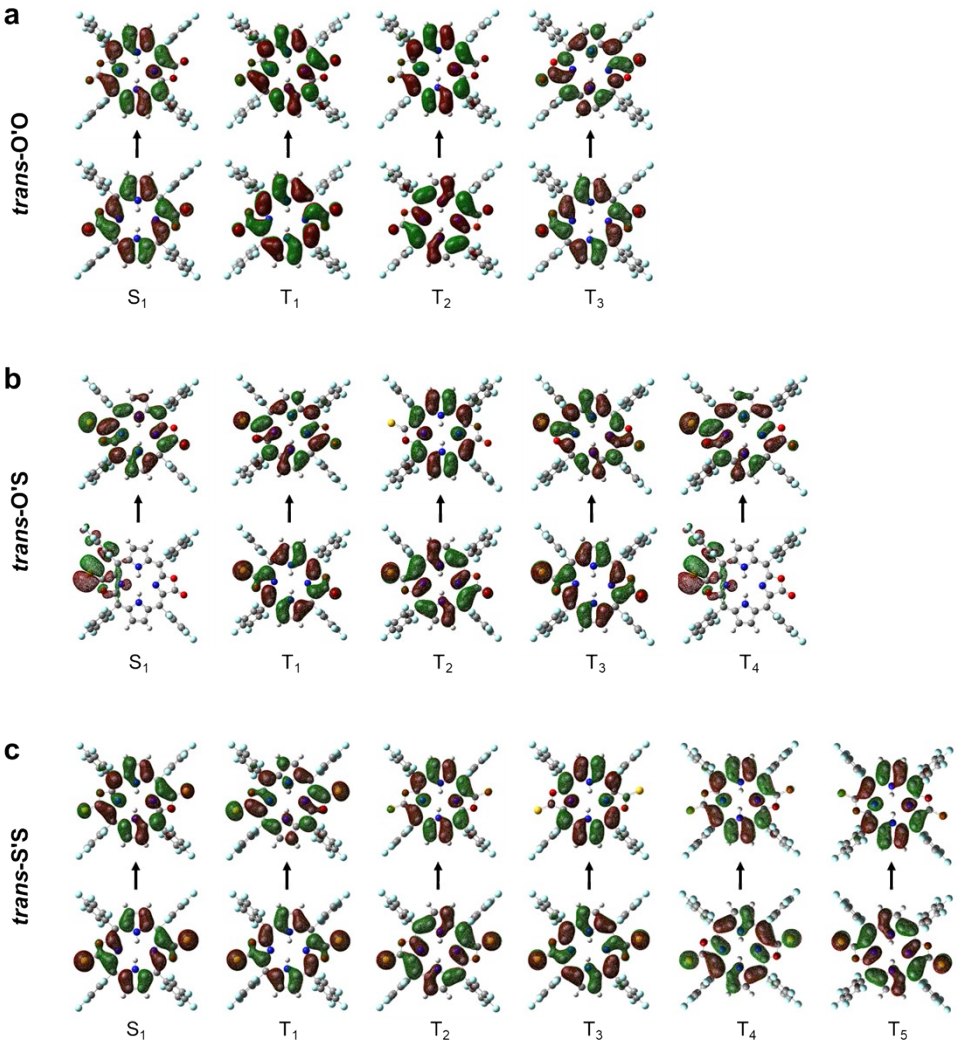

Figure S20. The frontier molecular orbitals of porphodilactone derivatives (***trans*-O'O**, ***trans*-O'S**, and ***trans*-S'S**) in their singlet states (S_1) and triplet states (T_1–T_n).

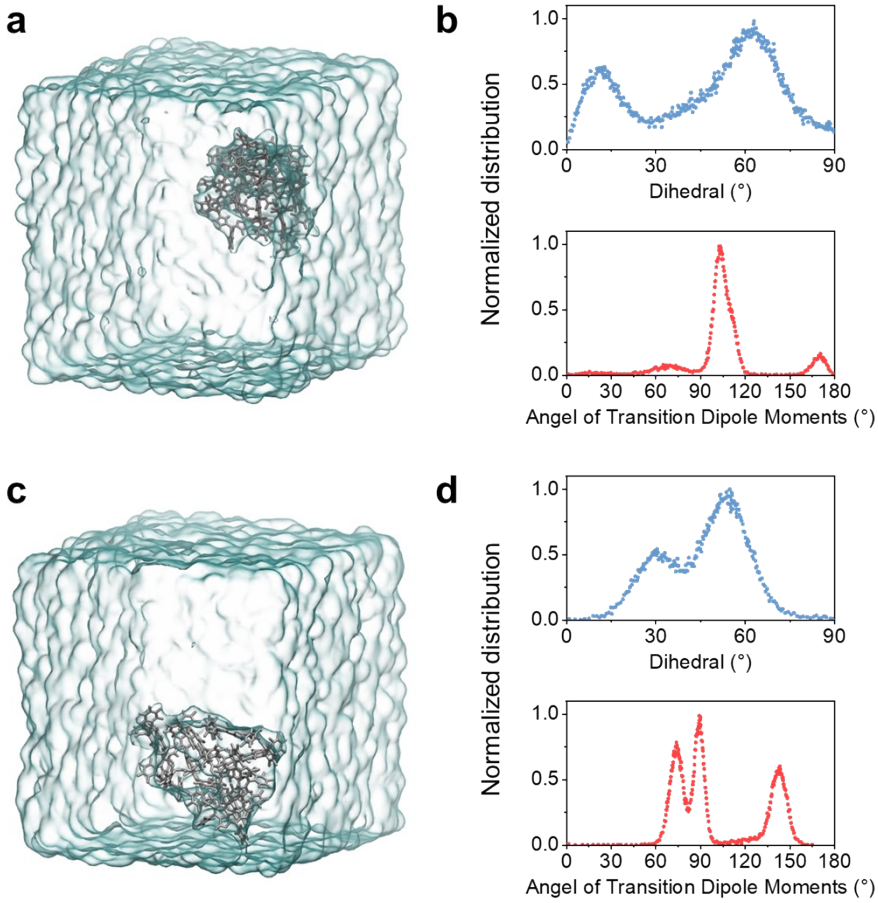

Figure S21. (a) Schematic illustration of the molecular aggregation of ***cis*-O'O** expected to pertain in nanoparticles as deduced from equilibrated MD simulations in a water box (50 × 50 × 50 Å). (b) Normalized distribution of dihedral and transition dipole moments angle between ***cis*-O'O** dimers. (c) Schematic illustration of the molecular aggregation of ***cis*-O'S** expected to pertain in nanoparticles as deduced from equilibrated MD simulations in a water box (50 × 50 × 50 Å). (d) Normalized distribution of dihedral and transition dipole moments angle between ***cis*-O'S** dimers.

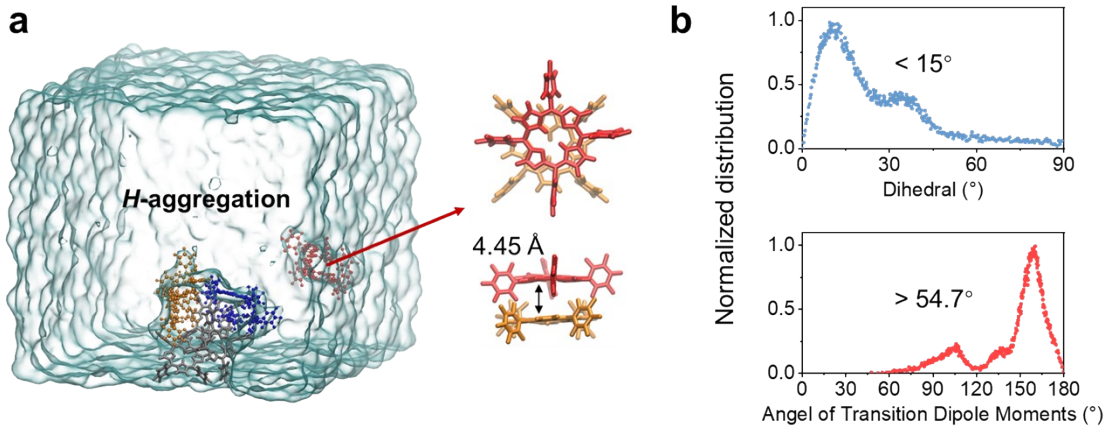

Figure S22. (a) Schematic illustration of the molecular aggregation of ***trans*-O'O** expected to pertain in nanoparticles as deduced from equilibrated MD simulations in a water box (50 × 50 × 50 Å). (b) Normalized distribution of dihedral and transition dipole moments angle between ***trans*-O'O** dimers.

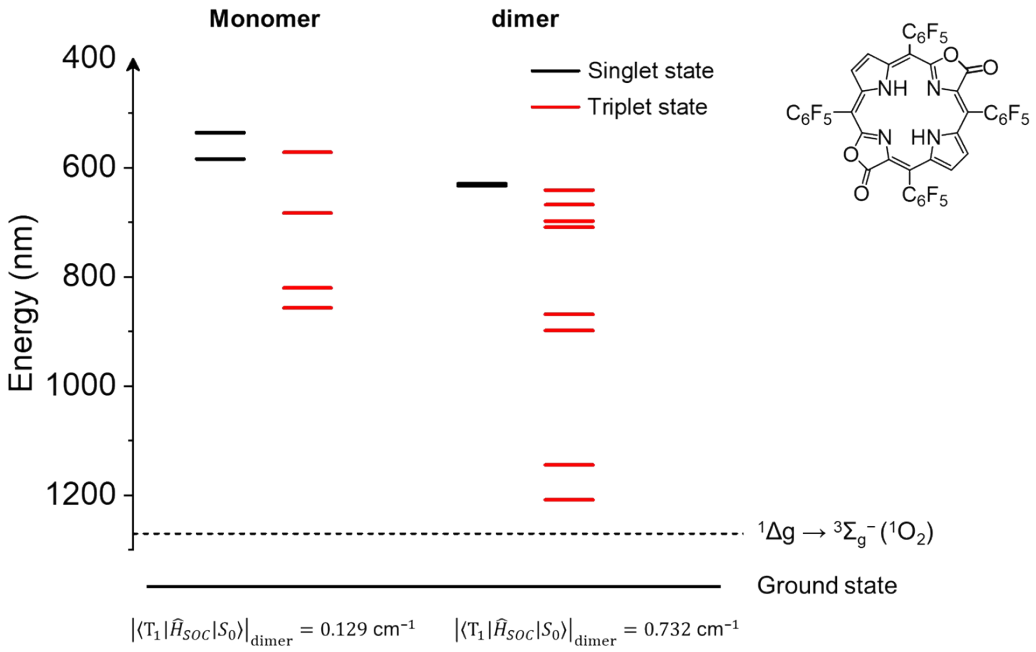

Figure S23. TD-DFT calculated energy-level diagrams and SOC parameters of excited triplet states of ***cis*-O'O** monomer and dimer structures.

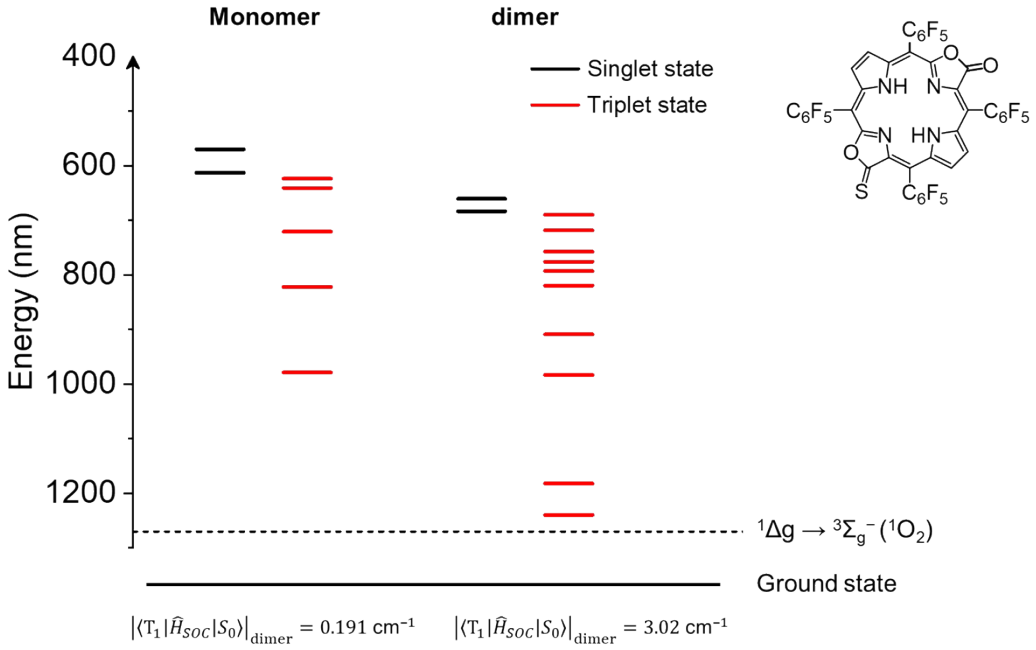

Figure S24. TD-DFT calculated energy-level diagrams and SOC parameters of excited triplet states of ***cis*-O'S** monomer and dimer structures.

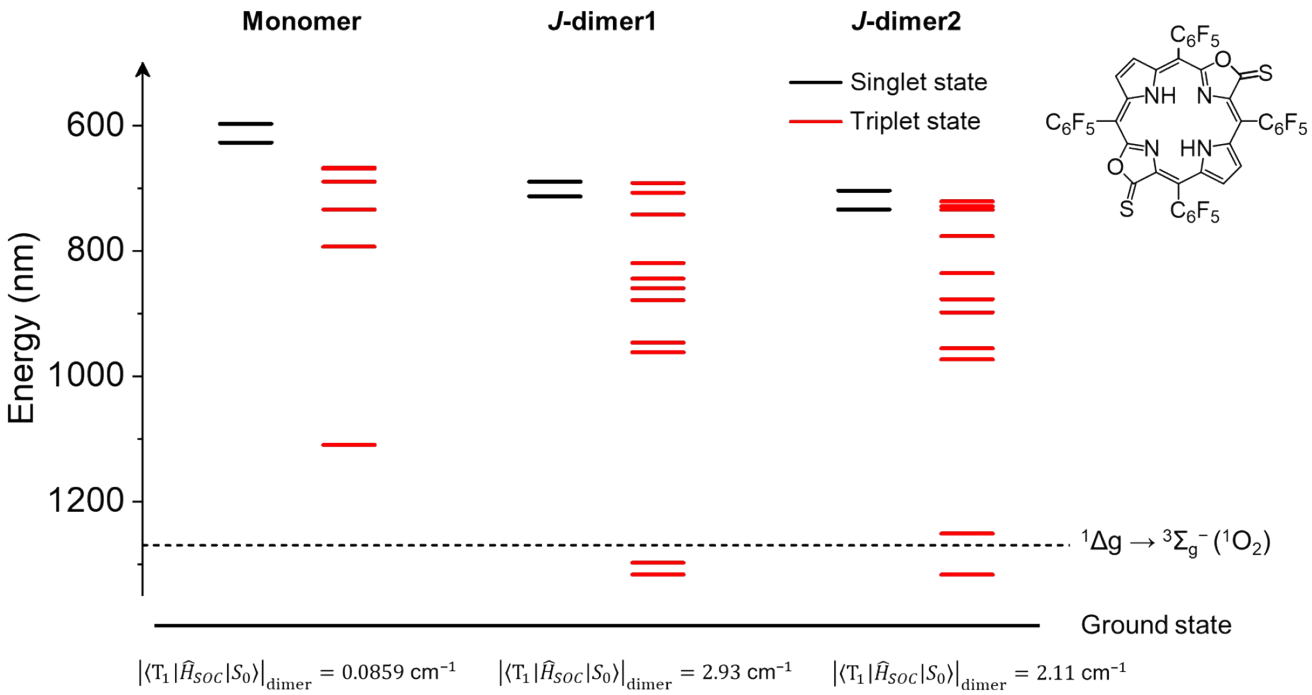

Figure S25. TD-DFT calculated energy-level diagrams and SOC parameters of excited triplet states of ***cis*-S'S** monomer and dimer structures.

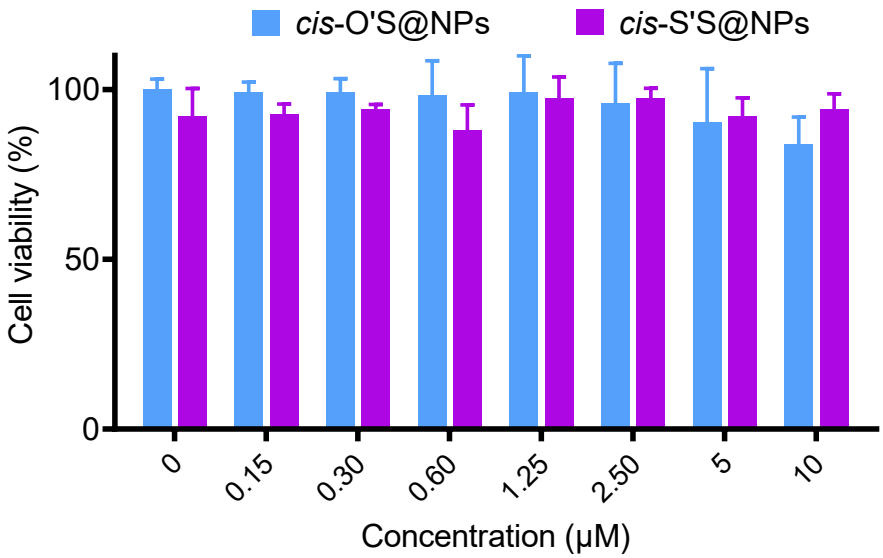

Figure S26. Dark-cytotoxicity of ***cis*-O'S@NPs** and ***cis*-S'S@NPs** (0−10 μM) on HeLa cells obtained by CCK-8 assay.

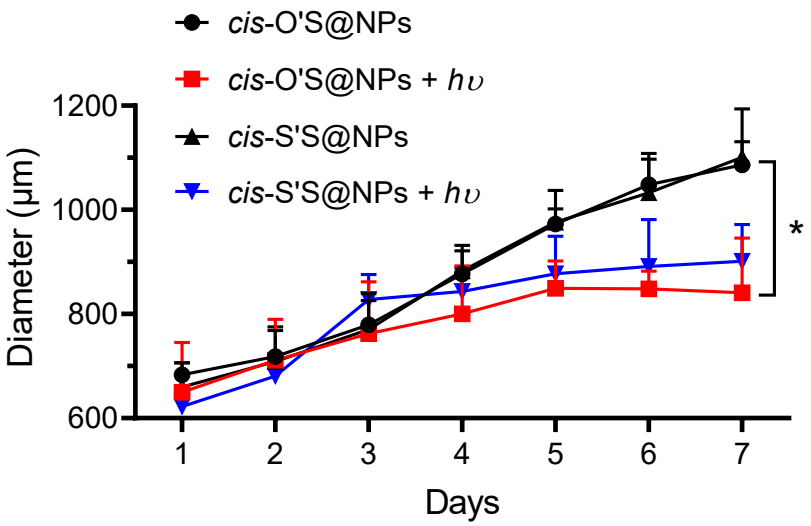

Figure S27. Diameter variation curves for MCSs treated with ***cis*-O'S@NPs** or ***cis*-S'S@NPs** under dark and light conditions (n = 3). *p < 0.05.

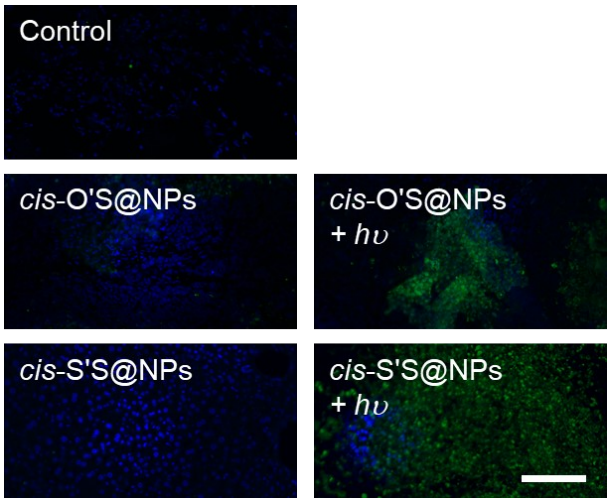

Figure S28. Analysis of tumor cell apoptosis by TUNEL assay for the different groups (Control, ***cis*-O'S@NPs**, ***cis*-S'S@NPs**, ***cis*-O'S@NPs** + *hυ*, and ***cis*-S'S@NPs** + *hυ*). Scale bar: 100 μm.

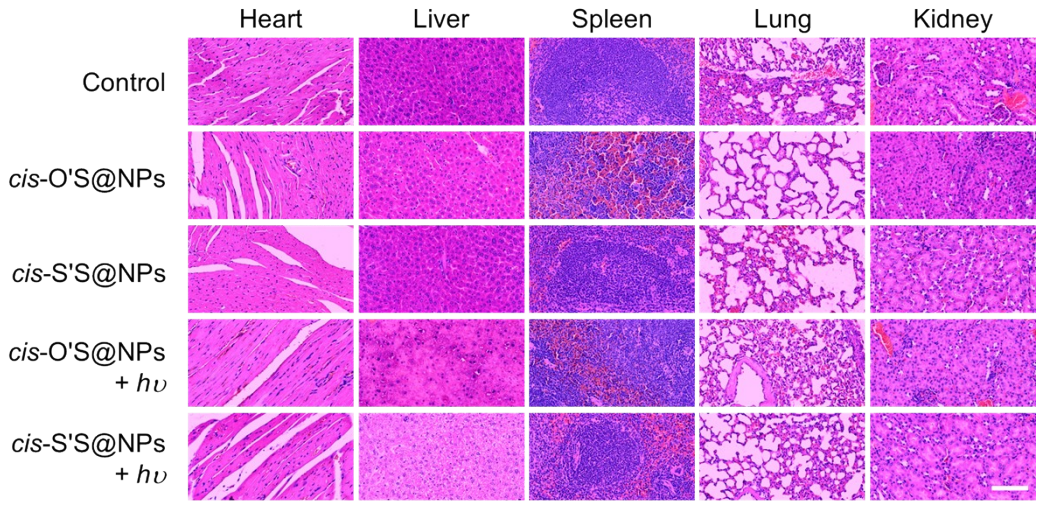

Figure S29. H&E staining images of major organs (heart, liver, spleen, lung, and kidney) taken from mice in the different treatment groups. Scale bar: 100 μm.

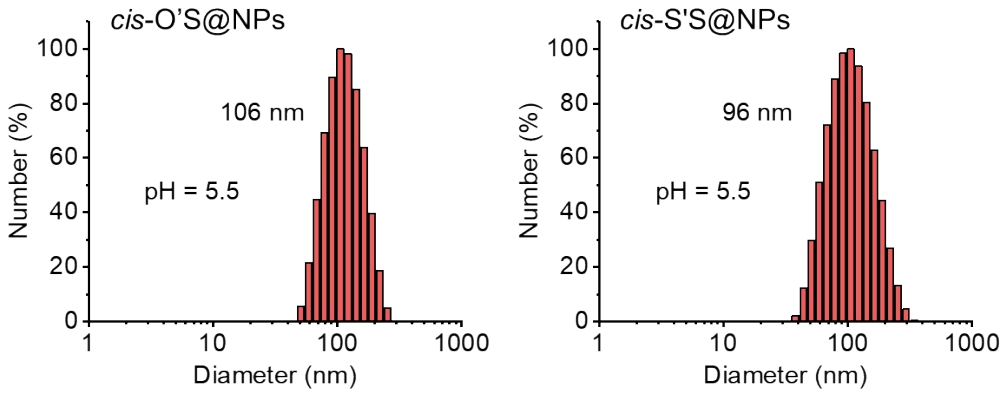

Figure S30. Size distributions of ***cis*-O'S@NPs** and ***cis*-S'S@NPs** obtained by DLS in a buffer solution with a pH value of 5.5.

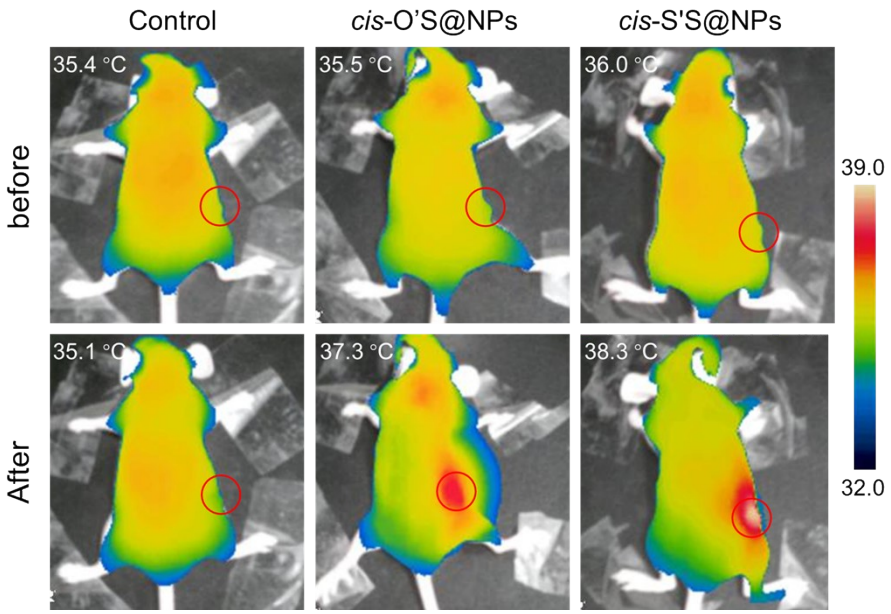

Figure S31. Infrared thermographs of the mice in control (PBS), ***cis*-O'S@NPs**, and ***cis*-S'S@NPs** groups before and after a 700 nm LED light irradiation for 10 mins (200 mW/cm^2).

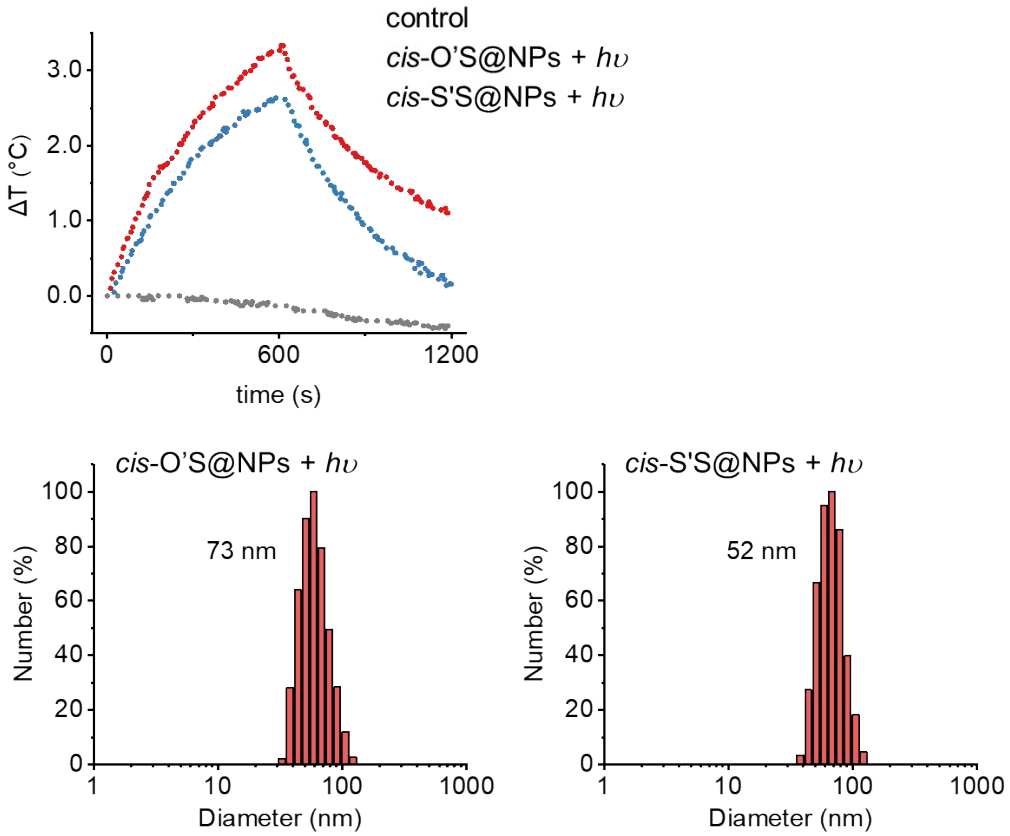

Figure S32. Temperature elevation curves and size distributions of ***cis*-O'S@NPs** and ***cis*-S'S@NPs** in aqueous solution (A_{700} = 0.5) subject to LED irradiation (700 nm, 0.2 W/cm^2).

References

[1] J.-Y. Hu, Z.-Y. Wu, K. Chai, Z.-S. Yang, Y.-S. Meng, Y. Ning, J. Zhang, J.-L. Zhang, *Inorg. Chem. Front.* **2017**, *4*, 1539-1545.

[2] D. J. Quimby, F. R. Longo, *J. Am. Chem. Soc.* **1975**, *97*, 5111-5117.

[3] R. Schmidt, E. Afshari, *J. Chem. Phys.* **1990**, *94*, 4377-4378.

[4] R. W. Redmond, J. N. Gamlin, *Photochem. Photobiol.* **1999**, *70*, 391-475.

[5] W. Jakubowski, *Cell Biol. Int.* **2000**, *24*, 757-760.

[6] J. Geng, Y. Zhang, Q. Gao, K. Neumann, H. Dong, H. Porter, M. Potter, H. Ren, D. Argyle, M. Bradley, *Nat. Chem.* **2021**, *13*, 805-810.

[7] A. D. Becke, *J. Chem. Phys.* **1993**, *98*, 5648-5652.

[8] M. J. Frisch, G. W. Trucks, H. B. Schlegel, G. E. Scuseria, M. A. Robb, J. R. Cheeseman, G. Scalmani, V. Barone, G. A. Petersson, H. Nakatsuji, X. Li, M. Caricato, A. V. Marenich, J. Bloino, B. G. Janesko, R. Gomperts, B. Mennucci, H. P. Hratchian, J. V. Ortiz, A. F. Izmaylov, J. L. Sonnenberg, Williams, F. Ding, F. Lipparini, F. Egidi, J. Goings, B. Peng, A. Petrone, T. Henderson, D. Ranasinghe, V. G. Zakrzewski, J. Gao, N. Rega, G. Zheng, W. Liang, M. Hada, M. Ehara, K. Toyota, R. Fukuda, J. Hasegawa, M. Ishida, T. Nakajima, Y. Honda, O. Kitao, H. Nakai, T. Vreven, K. Throssell, J. A. Montgomery Jr., J. E. Peralta, F. Ogliaro, M. J. Bearpark, J. J. Heyd, E. N. Brothers, K. N. Kudin, V. N. Staroverov, T. A. Keith, R. Kobayashi, J. Normand, K. Raghavachari, A. P. Rendell, J. C. Burant, S. S. Iyengar, J. Tomasi, M. Cossi, J. M. Millam, M. Klene, C. Adamo, R. Cammi, J. W. Ochterski, R. L. Martin, K. Morokuma, O. Farkas, J. B. Foresman, D. J. Fox, Gaussian, Inc., Wallingford, CT, **2016**.

[9] P. C. Hariharan, J. A. Pople, *Theor. Chim. Acta.* **1973**, *28*, 213-222.

[10] A. V. Marenich, C. J. Cramer, D. G. Truhlar, *J. Phys. Chem. B* **2009**, *113*, 6378-6396.

[11] S. G. Chiodo, M. Leopoldini, *Comput. Phys. Commun.* **2014**, *185*, 676-683.

[12] Y. Niu, W. Li, Q. Peng, H. Geng, Z. Shuai, *Mol. Phys.* **2018**, *116*, 1-13.

[13] D. Case, I. Ben-Shalom, S. Brozell, D. Cerutti, T. Cheatham III, V. Cruzeiro, T. Darden, R. Duke, D. Ghoreishi, M. Gilson, H. Gohlke, A. W. Goetz, D. Greene, R. Harris, N. Homeyer, Y. Huang, S. Izadi, A. Kovalenko, T. Kurtzman, T. S. Lee, S. LeGrand, P. Li, C. Lin, J. Liu, T. Luchko, R. Luo, D. J. Mermelstein, K. M. Merz, Y. Miao, G. Monard, C. Nguyen, H. Nguyen, I. Omelyan, A. Onufriev, F. Pan, R. Qi, D. R. Roe, A. Roitberg, C. Sagui, S. Schott-Verdugo, J. Shen, C. L. Simmerling, J. Smith, R. Salomon Ferrer, J. Swails, R. C. Walker, J. Wang, H. Wei, R. M. Wolf, X. Wu, L. Xiao, D. M. York, P. A. Kollm, AMBER 2018, University of California, San Francisco, **2018**.

[14] J. Wang, R. M. Wolf, J. W. Caldwell, P. A. Kollman, D. A. Case, *J. Comput. Chem.* **2004**, *25*, 1157-1174.